

Power Adaptive Network Coding for a Non-Orthogonal Multiple-Access Relay Channel

Sha Wei, Jun Li, Wen Chen, Hang Su, Zihuai Lin, and Branka Vucetic

Abstract

In this paper we propose a novel power adapted network coding (PANC) for a non-orthogonal multiple-access relay channel (MARC), where two sources transmit their information simultaneously to the destination with the help of a relay. Different from the conventional XOR-based network coding (CXNC), the relay in our PANC generates network coded bits by considering the coefficients of the source-to-relay channels, and forwards each bit with a pre-optimized power level. Specifically, by defining a symbol pair as two symbols from the two sources, we first derive the exact symbol pair error rate (SPER) of the system. Noting that the generations of the exact SPER are complicated due to the irregularity of the decision regions caused by random channel coefficients, we propose a coordinate transform (CT) method to simplify the derivations of the SPER. Next, we prove that with a power scaling factor at relay, our PANC scheme can achieve full diversity gain, i.e., two-order diversity gain, of the system, while the CXNC can only achieve one-order diversity gain due to multi-user interference. In addition, we optimize the power levels at the relay to equivalently minimize the SPER at the destination concerning the relationship between SPER and minimum Euclidean distance of the received constellation. Simulation results show that (1) the SPER derived based on our CT method can well approximate the exact SPER with a much lower complexity; (2) the PANC scheme with power level optimizations and power scaling factor design can achieve full diversity, and obtain a much higher coding gain than the PANC scheme with randomly chosen power levels.

Index Terms – network coding, power optimization, multiple access relay channel, error probability

Sha Wei, Wen Chen and Hang Su are with Department of Electronic Engineering, Shanghai Jiaotong University, Shanghai, China, 200240, email: {venessa724, wenchen, Hmilyanjohn}@sjtu.edu.cn.

Jun Li, Zihuai Lin, and Branka Vucetic are with School of Electrical and Information Engineering, The University of Sydney, NSW, 2006, Australia. {jun.li1,zihuai.lin,branka.vucetic}@sydney.edu.au

I. INTRODUCTION

Relaying techniques have been studied for decades to improve the reliability of wireless networks by exploiting spatial diversity via intermediate relay nodes [1], [2], [3]. Network coding, on the other hand, originated from wire-line networks [4], [5], has been recently leveraged to the wireless networks to enhance the network throughput [6]. With the implementations of diversity techniques and network coding at the relay nodes, it is anticipated that the wireless networks can achieve a more reliable communication with a higher network throughput.

Wireless networks can take the advantage of the broadcast nature of wireless signals to further increase the throughput. For instance, by allowing multiple sources transmit in the same channel, less transmissions are needed, and thus a larger network throughput is achieved. However, this kind of non-orthogonal transmissions will lead to multi-user interferences, which could jeopardize the system error performance. Many wireless network coding schemes are designed with the considerations of multi-user interference issue in non-orthogonal transmissions [7], [8], [9], [10], [11]. In [7], an optimal network coded relay function is derived to minimize the bit error rate in a non-orthogonal two-way relay channel (TWRC). In [8], physical-layer network coding is proposed in a non-orthogonal TWRC, where the relay maps the interfered signals from the two sources to a network coded digit. In [9], [10], [11], denoise-and-forward based network coding schemes are designed for the TWRC with multi-user interferences.

More practical than the TWRC, multiple access relay channel (MARC) has been recognized as a fundamental building block for cellular networks and wireless sensor networks. Different from the TWRC, where perfect side information, i.e., each source's own information, is available at each receiver side, the MARC only has imperfect information at the destination from the sources. The MARC model has attracted a large amount of research interest from both academic and industrial communities [12], [13], [14], [15], [16], [17], [18]. In [14], Galois field network coding is designed to achieve the full diversity gain of the MARC. In [15], the authors propose a frame-wise binary field network coding which enables belief propagation decoding at the destination to achieve the full diversity gain and a high coding gain. However, we note that most of these works consider orthogonal MARC, where multiple sources transmit their signals by using time-division multiple access or frequency-division multiple access manners. Multi-user interferences are not considered in these works, which simplifies the network coding design but leads to a lower spectrum efficiency.

In this paper, we are interested in designing novel network coding schemes for a non-orthogonal MARC over fading channels to achieve the full diversity gain and a good coding gain. Although the conventional CXNC has been shown to achieve full diversity in the orthogonal MARC [14], we will prove that it cannot achieve full diversity gain in a non-orthogonal one due to multi-user interferences. Specifically in this paper, we consider a two-source, one-relay, one destination non-orthogonal MARC.

There are three major concerns and contributions in our network coding design. First is how to achieve the full diversity gain in the MARC. We propose a novel power adapted network coding (PANC). Different from the CXNC, the relay in our PANC generates network coded bits by considering the coefficients of the source-to-relay channels, and forwards each bit with one of the two given power levels of the relay. Based on the received signals, the relay decides which power level should be applied to each network coded bit. We prove that our PANC scheme with the design of power scaling at relay can achieve the full diversity gain, i.e., two-order diversity gain, of the system, while the CXNC scheme can only achieve one-order diversity gain with or without power scaling design at relay due to multi-user interference.

Secondly, we derive the exact error probability at the destination. By defining a symbol pair as two symbols from the two sources, we develop the exact symbol pair error rate (SPER), with the setup of received constellations at both the relay and the destination. Due to the geometry property of the decision regions, we adopt the wedge probability computation method to investigate the SPER. The wedge probability computation method was first introduced in [19] to compute error probability with wedge-shaped decision region in a polar coordinate. Noting that the derivations of the exact SPER are complicated due to the irregularity of the decision regions caused by random channel coefficients, we propose a coordinate transform (CT) method to simplify the derivations. In the CT method, we transform the original parallelogram geometry to a rectangle and approximate the exact results based on original constellation with simple expressions.

Thirdly, we optimize the two power adaption levels at the relay to achieve a higher coding gain. Note that there are quite a few works on the optimizations of the relay transmissions to enhance the error performance over fading channels. In [20], soft information scheme is proposed in fading channels to reduce the error propagation by controlling the transmission power at the relay. However, this scheme is not practical as the optimized power at the relay is a continuous variable. In this paper, we will minimize the SPER by optimizing the two power adaption levels. Specifically, we propose a criteria based on the relationship between Euclidean distance and

the SPER, and formulate a convex optimization problem to develop the optimal power adaption levels at the relay.

Simulation results show that (1) the SPER derived based on our CT method can well approximate the exact SPER with a much lower complexity; (2) the PANC scheme with power level optimizations and power scaling factor design can achieve full diversity, and obtain a much higher coding gain than the PANC scheme with randomly chosen power levels; (3) the CXNC scheme cannot achieve full diversity with or without the power scaling design.

The rest of this paper is organized as follows. We first describe the system model in Section II and propose the PANC scheme in Section III. Then we develop the exact system SPER and its approximation in Section IV. In Section V, we address the error propagation problem, and formulate and solve the optimization problem by minimizing the system SPER. Simulation results are presented in Section VI, and conclusions are drawn in Section VII.

The notations used in this work are as follows. \Re and \Im respectively denote the real and the imaginary parts of a complex number. Denote a ray by l_{ij} where the subscript ij is the label of the line. Denote AB a line segment and \overline{AB} the length between points A and B , respectively. We use the format *ray-vertex-ray* and *ray-vertex-vertex-ray* to describe a wedge and wedge combination, respectively. Denote $\phi = \angle ABC$ as the crossing angle between line segment AB and BC with the intersection point B . The one-dimensional Q-function is defined as $Q_1(x) = \frac{1}{\pi} \int_0^{\frac{\pi}{2}} \exp\left(-\frac{x^2}{2\sin^2\theta}\right) d\theta$. The two-dimensional Q-function $Q_2(x, y; \rho)$ with $x = y$ is simplified as $Q_2(x; \rho)$ with expression $Q_2(x; \rho) = \frac{1}{\pi} \int_0^{\arctan\left(\sqrt{\frac{1+\rho}{1-\rho}}\right)} \exp\left(-\frac{x^2}{2\sin^2\phi}\right) d\phi$.

II. SYSTEM MODEL

Consider a two-source single-relay multiple-access relaying system, where two sources \mathcal{S}_1 and \mathcal{S}_2 transmit their information to the common destination \mathcal{D} with the assistance of a half-duplex relay node \mathcal{R} . Each transmission period is divided into two transmission phases. In the first transmission phase, the two sources simultaneously broadcast their symbols x_1 and x_2 to both the destination and the relay. In the second transmission phase, the two sources keep silent, while the relay processes the received signals and forwards the network coded symbol $x_{\mathcal{R}}$ to the destination. At the end of the second phase, the destination decodes the two sources' information based on the received signals.

We assume that all the transmitted signals are binary phase shift keying (BPSK) modulated with equal probability, i.e., $x_1, x_2, x_{\mathcal{R}} \in \{\pm 1\}$, and all the signals are transmitted in the same

frequency band. The channel between any two given nodes j and k , $j \in \{1, 2, \mathcal{R}\}$, $k \in \{\mathcal{R}, \mathcal{D}\}$, and $j \neq k$, is denoted by h_{jk} with the subscripts indicating the nodes under consideration. We assume that h_{jk} for all the j and k are Rayleigh distributed with zero mean and variance $\bar{\gamma}_{jk}$. We consider slow fading channels in our system, i.e., the channels are constant during a transmission period, while independently change from one transmission period to another.

Also, we implement the channel phase pre-equalization for both the source-to-destination multiple access channels (MAC) and the relay-to-destination channel before each transmission. Thus, the effective source-to-destination and relay-to-destination channel coefficients can be regarded as real-valued channels, i.e., real channel coefficients and real values of noise samples.¹

Based on the aforementioned system settings and assumptions, the received signals at the relay and destination in the first transmission phase can be written as

$$\begin{aligned} y_{\mathcal{R}} &= \sqrt{E_1}h_{1\mathcal{R}}x_1 + \sqrt{E_2}h_{2\mathcal{R}}x_2 + n_{\mathcal{R}}, \\ y_1 &= \sqrt{E_1}|h_{1\mathcal{D}}|x_1 + \sqrt{E_2}|h_{2\mathcal{D}}|x_2 + n_1, \end{aligned} \quad (1)$$

respectively, where E_1 and E_2 denote the transmission power of \mathcal{S}_1 , \mathcal{S}_2 , respectively, $n_{\mathcal{R}}$ is the complex additive white Gaussian noise (AWGN) sample at the relay with zero mean and variance $\sigma^2/2$ per dimension, and n_1 is the real AWGN sample at the destination with zero mean and variance σ^2 .

As we adopt the joint power scaling and adaption scheme at the relay, the instantaneous power at the relay is optimized given the channel realization within each transmission period tending to minimize the SER and achieve full diversity at the destination. Specifically, in the power scaling, we have the scaling factor α ($0 \leq \alpha \leq 1$) which is determined based on the channel conditions. In the power adaption, we have two power levels, namely, a and b . We have $a^2 + b^2 \leq 2E_{\mathcal{R}}^{\text{ave}}$, where $E_{\mathcal{R}}^{\text{ave}}$ is denoted as the average transmission power at the relay. The determinations of α , a , b will be discussed latter in details. Therefore, in the second transmission phase, the received signal at destination can be expressed as

$$y_2 = \sqrt{\alpha E_{\mathcal{R}}}|h_{\mathcal{R}\mathcal{D}}|x_{\mathcal{R}} + n_2, \quad (2)$$

where n_2 is the real AWGN at destination with zero mean and variance σ^2 , and $E_{\mathcal{R}} \in \{a, b\}$ represents the adaptive power level.

¹Note that, without channel phase pre-equalization, we will encounter a four-dimensional received constellation at destination, namely, the real and imaginary parts of received signal in the first phase, and the real and imaginary parts of received signal in the second phase, respectively, which leave the exact error probability analysis hardly derivable.

III. NETWORK CODED POWER ADAPTION SCHEME AT RELAY

In the conventional CXNC based MARC, XOR operations are implemented at the relay on the two sources' information. We will show later in Section V that the system cannot achieve full diversity with the conventional network coding. To solve this problem, we propose the PANC scheme, which also take account the source-to-relay channels in network coding design.

Firstly, the relay obtain the two sources' information (x_1, x_2) from its received signal $y_{\mathcal{R}}$ by utilizing the maximum likelihood (ML) detection, i.e.,

$$(\hat{x}_1, \hat{x}_2) = \arg \min_{\tilde{x}_1, \tilde{x}_2 \in \{\pm 1\}} \left| y_{\mathcal{R}} - \sqrt{E_{1\mathcal{R}}} h_{1\mathcal{R}} \tilde{x}_1 - \sqrt{E_{2\mathcal{R}}} h_{2\mathcal{R}} \tilde{x}_2 \right|^2, \quad (3)$$

where $(\hat{\cdot})$ denotes the detected symbol, and $(\tilde{\cdot})$ denotes the trial symbol used in the hypothesis-detection problem. Then the relay takes network coding operation on the two detected symbols. The network coded operation in our PANC is denoted by \boxplus , which is different from the conventional XOR operation. That is, we calculate $x_{\mathcal{R}}$ by $x_{\mathcal{R}} = \hat{x}_1 \boxplus \hat{x}_2 = \text{sign}(|h_{1\mathcal{R}}| \hat{x}_1 + |h_{2\mathcal{R}}| \hat{x}_2)$. Next, the relay chooses the power level $E_{\mathcal{R}}$ based on the decoded symbols, i.e., if $(\hat{x}_1 = 1, \hat{x}_2 = 1)$ or $(\hat{x}_1 = -1, \hat{x}_2 = -1)$, power level is chosen as a ; else if $(\hat{x}_1 = 1, \hat{x}_2 = -1)$ or $(\hat{x}_1 = -1, \hat{x}_2 = 1)$, power level is chosen as b . The reason for adopting the new proposed network coding operation and power level allocation method is that the received constellation at destination is a parallelogram, on which the $(\hat{x}_1 = 1, \hat{x}_2 = 1)$ corresponding constellation point lies in a diagonal with the $(\hat{x}_1 = -1, \hat{x}_2 = -1)$ corresponding constellation point. While for XOR operation, the received constellation is an irregular quadrilateral no matter what power level allocation result we implement.

The values of a and b are optimized by minimizing the system SPER at the destination. Suppose that the instantaneous channel state information (CSI) of the MARC is available to the destination before the transmission period starts. The destination first optimizes the power levels a and b by minimizing the instantaneous SPER based on the CSI, and then feedbacks the values to the relay before the transmission period starts. The relay will use this power adaption to transmit the network coded symbol $x_{\mathcal{R}}$. Note that, as the values of a and b is derived based on the instantaneous CSI, their values will keep invariant within each transmission period, and change from one transmission period to another.

The PANC scheme at the relay can also be illustrated by a two-dimensional instantaneous relay constellation (IRC), which is associated with the SPER calculation in the next section. The

signal part of $y_{\mathcal{R}}$, i.e., $\sqrt{E_1}h_{1\mathcal{R}}x_1 + \sqrt{E_2}h_{2\mathcal{R}}x_2$, can be seen as a point in the IRC with X-axis being its real part, and Y-axis being its imaginary part. We define the constellation points (CPs) V_i of the IRC, $i = 1, \dots, 4$, to represent the four possible values of $\pm\sqrt{E_1}h_{1\mathcal{R}} \pm \sqrt{E_2}h_{2\mathcal{R}}$, and define the sources' symbol pairs by $T_i \triangleq (x_1, x_2)$. Specifically, we have $T_1 \triangleq (1, 1)$, $T_2 \triangleq (-1, 1)$, $T_3 \triangleq (1, -1)$, and $T_4 \triangleq (-1, -1)$.

From Fig. 1, we can see that the geometry of the IRC composed by CPs V_i is a parallelogram. Similar to Voronoi diagram in [21], the decision regions are segmented by the perpendicular bisectors of each side of the parallelogram. Specifically, rays l_{12} , l_{13} , l_{24} and l_{34} are perpendicular bisectors of sides V_1V_2 , V_1V_3 , V_2V_4 and V_3V_4 , respectively, M_1 is the crossing points of rays l_{12} and l_{13} , and M_2 is the crossing points of rays l_{24} and l_{34} . M_{ij} is the middle point of each side V_iV_j . The decision region Ω_{V_1} of V_1 , defined as wedge $l_{12} - M_1 - l_{13}$ in Fig 1, is given by

$$\Omega_{V_1} \triangleq \left\{ \begin{aligned} &\frac{\Re\{h_{2\mathcal{R}}\}}{\Im\{h_{2\mathcal{R}}\}}\Re\{y_{\mathcal{R}}\} + \Im\{y_{\mathcal{R}}\} - \Im\{h_{1\mathcal{R}}\} - \frac{\sqrt{E_1}\Re\{h_{1\mathcal{R}}\}\Re\{h_{2\mathcal{R}}\}}{\Im\{h_{2\mathcal{R}}\}} < 0 \cap \\ &\frac{\Re\{h_{1\mathcal{R}}\}}{\Im\{h_{1\mathcal{R}}\}}\Re\{y_{\mathcal{R}}\} + \Im\{y_{\mathcal{R}}\} - \Im\{h_{2\mathcal{R}}\} - \frac{\sqrt{E_2}\Re\{h_{1\mathcal{R}}\}\Re\{h_{2\mathcal{R}}\}}{\Im\{h_{1\mathcal{R}}\}} \geq 0 \end{aligned} \right\}. \quad (4)$$

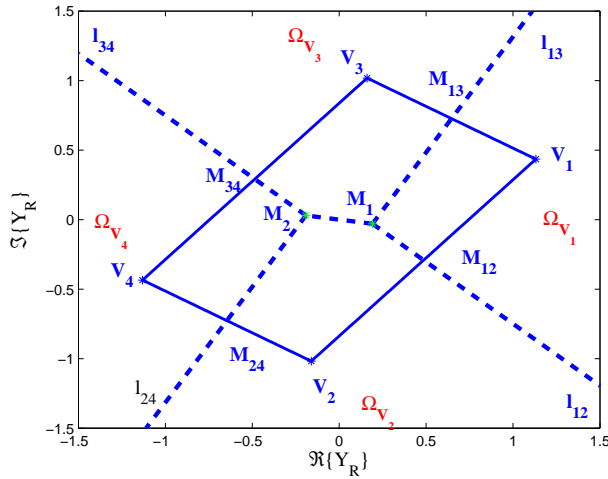


Fig. 1: One possible instantaneous relay constellation, where dashed lines represent boundaries of decision regions.

Similarly, we can obtain the decision regions of V_2 , V_3 and V_4 , denoted by Ω_{V_2} , Ω_{V_3} , and Ω_{V_4} , respectively. Based on the four decision regions, we have the one-to-one mapping between the

CPs and the network coded power level as

$$\sqrt{E_{\mathcal{R}}}x_{\mathcal{R}} = \begin{cases} a & \text{if } (\Re\{y_{\mathcal{R}}\}, \Im\{y_{\mathcal{R}}\}) \in \Omega_{V_1}, \\ b & \text{if } (\Re\{y_{\mathcal{R}}\}, \Im\{y_{\mathcal{R}}\}) \in \Omega_{V_2}, \\ -b & \text{if } (\Re\{y_{\mathcal{R}}\}, \Im\{y_{\mathcal{R}}\}) \in \Omega_{V_3}, \\ -a & \text{if } (\Re\{y_{\mathcal{R}}\}, \Im\{y_{\mathcal{R}}\}) \in \Omega_{V_4}, \end{cases} \quad (5)$$

Based on the observations y_1 and y_2 , the destination jointly decode the two source symbols with the minimum Euclidean distance detection. Then we have

$$(\hat{x}_1, \hat{x}_2) = \arg \min_{\tilde{x}_1, \tilde{x}_2 \in \{\pm 1\}} \left(\left| y_1 - \sum_{j=1}^2 |h_{j\mathcal{D}}| \tilde{x}_j \right|^2 + \left| y_2 - |h_{\mathcal{R}\mathcal{D}}| \sqrt{\tilde{E}_{\mathcal{R}}} (\tilde{x}_1 \boxplus \tilde{x}_2) \right|^2 \right), \quad (6)$$

where $\tilde{E}_{\mathcal{R}} \in \{a, b\}$ is determined by \tilde{x}_1 and \tilde{x}_2 .

IV. ERROR PERFORMANCE ANALYSIS

In this section, we investigate the instantaneous SPER performance of the PANC given a channel realization vector $\mathbf{h} = [h_{1\mathcal{R}}, h_{2\mathcal{R}}, h_{1\mathcal{D}}, h_{2\mathcal{D}}, h_{\mathcal{R}\mathcal{D}}]$. Assuming symbols are transmitted with equal probability, then the general expression of the system SPER of the PANC scheme is given by

$$P_{e,inst} = \sum_{i=1}^4 P(\mathcal{E}|T_i, \mathbf{h})P(T_i) = \frac{1}{4} \sum_{i=1}^4 P(\mathcal{E}|T_i, \mathbf{h}), \quad (7)$$

where T_i is the symbol pair defined in Section III, \mathcal{E} denotes the symbol error event at the destination that a transmitted symbol pair from two sources is decoded to an erroneous pair, i.e., either x_1 or x_2 is wrongly detected or both x_1 and x_2 are wrongly detected, $P(\mathcal{E}|T_i, \mathbf{h})$ is the conditional SPER given T_i is transmitted and the channel realization \mathbf{h} , and $P(T_i) = \frac{1}{4}$ is the probability that T_i is sent by the two sources. Since the decision regions of T_1 and T_4 are symmetric, and the decision regions of T_2 and T_3 are symmetric, we have $P(\mathcal{E}|T_1) = P(\mathcal{E}|T_4)$ and $P(\mathcal{E}|T_2) = P(\mathcal{E}|T_3)$. Therefore, (7) can be rewritten as

$$\begin{aligned} P_{e,inst} &= \frac{1}{2} (P(\mathcal{E}|T_1, \mathbf{h}) + P(\mathcal{E}|T_2, \mathbf{h})) \\ &= \frac{1}{2} \left\{ \sum_{i=1}^2 \sum_{k \in \{\pm a, \pm b\}} P(\mathcal{E}|k, T_i, h_{1\mathcal{D}}, h_{2\mathcal{D}}, h_{\mathcal{R}\mathcal{D}}) P(\sqrt{E_{\mathcal{R}}}x_{\mathcal{R}} = k|T_i, h_{1\mathcal{R}}, h_{2\mathcal{R}}) \right\}, \end{aligned} \quad (8)$$

where $P(\sqrt{E_{\mathcal{R}}}x_{\mathcal{R}} = k|T_i, h_{1\mathcal{R}}, h_{2\mathcal{R}})$ is the conditional probability that $x_{\mathcal{R}}$ is allocated to the power level $|k|$ at the relay, and $P(\mathcal{E}|k, T_i, h_{1\mathcal{D}}, h_{2\mathcal{D}}, h_{\mathcal{R}\mathcal{D}})$ is the conditional probability that the

destination makes a wrong decision on the sources' symbol pair T_i . For the sake of simplicity, we omit the channel coefficients in these notations, and use $P(\sqrt{E_{\mathcal{R}}}x_{\mathcal{R}} = k|T_i)$ and $P(\mathcal{E}|k, T_i)$.

In the following we will derive $P_{e,inst}$ based on two methods. The first method is based on wedge probability computation [19], [22], which derives the instantaneous SPER of the system. However, the calculations of various wedge probabilities are very complicated and time-consuming. Hence, we simplify the wedge probabilities by applying coordinate transformations with a little accuracy loss.

A. SPER based on Wedge Probabilities

We now investigate the SPER performance of the PANC scheme based on the wedge probability computation method. Due to the randomness of channel realizations, the two-dimension decision regions of a symbol pair T_i at both the relay and the destination are irregular and wedge-like, e.g., one possible case of the received constellation and its corresponding decision regions at the relay is shown in Fig. 1. We thus use the wedge probability computation method to facilitate the derivation of the SPER. There are totally five basic wedge prototypes, discussed in Appendix A. Corresponding to these five wedge prototypes, we derive the corresponding five wedge probabilities in Appendix A, i.e., P_{w_i} for $i \in \{1, \dots, 5\}$, based on which, we will later derive the SPER of the system.

We first focus on the probabilities $P(\sqrt{E_{\mathcal{R}}}x_{\mathcal{R}} = k|T_i)$, $k \in \{\pm a, \pm b\}$, at the relay. With the setup of IRC given in Section III, we calculate the probabilities that relay detects the received signal successfully, i.e., $P(\sqrt{E_{\mathcal{R}}}x_{\mathcal{R}} = a|T_1)$ and $P(\sqrt{E_{\mathcal{R}}}x_{\mathcal{R}} = b|T_2)$, by P_{w_4} and P_{w_5} defined in equations (37) and (38) respectively, and calculate the probabilities that relay makes wrong decisions, i.e., $P(\sqrt{E_{\mathcal{R}}}x_{\mathcal{R}} \in \{\pm b, -a\}|T_1)$ and $P(\sqrt{E_{\mathcal{R}}}x_{\mathcal{R}} \in \{\pm b, -a\}|T_2)$, by P_{w_1} , P_{w_2} , and P_{w_3} defined in equations (34), (35), and (36), respectively. The computation of exact instantaneous correct probabilities and error probabilities are divided into six cases according to the relative lengths and intersection angles of parallelogram's neighboring sides, and intersection

$$\begin{aligned}
P(\sqrt{E_{\mathcal{R}}}x_{\mathcal{R}} = a|T_1) &= P_{w_4} \left(d_{11}, \arcsin \left(\frac{\overline{V_1 M_{13}}}{\overline{V_1 M_1}} \right), \arcsin \left(\frac{\overline{V_1 M_{12}}}{\overline{V_1 M_1}} \right) \right), \\
P(\sqrt{E_{\mathcal{R}}}x_{\mathcal{R}} = b|T_1) &= P_{w_3}(d_{12}, d_{11}, \angle V_1 M_2 M_{24}, \pi - \angle V_1 M_2 M_1, \angle V_1 M_1 M_{12}, \angle V_1 M_1 M_2, 1, 1), \\
P(\sqrt{E_{\mathcal{R}}}x_{\mathcal{R}} = -b|T_1) &= P_{w_3}(d_{11}, d_{12}, \pi - \angle V_1 M_1 M_2, \pi - \angle V_1 M_1 M_{13}, \angle V_1 M_2 M_1, \angle V_1 M_2 M_{34}, 1, 1), \\
P(\sqrt{E_{\mathcal{R}}}x_{\mathcal{R}} = b|T_2) &= P_{w_5} \left(d_{21}, d_{22}, \pi - \arcsin \left(\frac{\overline{V_2 M_{12}}}{\overline{V_2 M_1}} \right), \arcsin \left(\frac{\overline{V_2 M_{24}}}{\overline{V_2 M_2}} \right), \angle M_1 V_2 M_2, \angle V_2 M_1 M_2 \right), \\
P(\sqrt{E_{\mathcal{R}}}x_{\mathcal{R}} = a|T_2) &= P_{w_2}(d_{21}, \angle V_2 M_1 M_{12}, \pi - \angle V_2 M_1 M_{13}), \\
P(\sqrt{E_{\mathcal{R}}}x_{\mathcal{R}} = -a|T_2) &= P_{w_2}(d_{21}, \angle V_2 M_1 M_{34}, \pi - \angle V_2 M_1 M_{13}).
\end{aligned} \tag{10}$$

angles of perpendicular bisectors. These six cases are given as

$$\left\{ \begin{array}{l} \overline{V_1 V_4} > \overline{V_2 V_3} \\ \overline{V_1 V_4} \leq \overline{V_2 V_3} \end{array} \right\} \left\{ \begin{array}{l} M_1, M_2 \notin \mathcal{P} \left\{ \begin{array}{l} \overline{V_1 V_2} > \overline{V_1 V_3}, \text{ Case one} \\ \overline{V_1 V_2} \leq \overline{V_1 V_3}, \text{ Case two} \end{array} \right. \\ M_1, M_2 \in \mathcal{P}, \text{ Case three} \\ M_1, M_2 \notin \mathcal{P} \left\{ \begin{array}{l} \overline{V_1 V_2} > \overline{V_1 V_3}, \text{ Case four} \\ \overline{V_1 V_2} \leq \overline{V_1 V_3}, \text{ Case five} \end{array} \right. \\ M_1, M_2 \in \mathcal{P}, \text{ Case six} \end{array} \right. \tag{9}$$

In (10), we show an example of computing $P(\sqrt{E_{\mathcal{R}}}x_{\mathcal{R}} = k|T_i)$ for Case three, i.e., $\overline{V_1 V_4} > \overline{V_2 V_3}$ and $M_1, M_2 \in \mathcal{P}$, where \mathcal{P} is defined as the region of parallelogram in IRC. Let d_{ik} be the normalized distance between V_i and M_k , which is given by $d_{ik} = \frac{|V_i - M_k|^2}{\sigma^2}$. According to the law of total probability, $P(\sqrt{E_{\mathcal{R}}}x_{\mathcal{R}} = -a|T_1) = 1 - \sum_{k \in \{a, \pm b\}} P(\sqrt{E_{\mathcal{R}}}x_{\mathcal{R}} = k|T_1)$ and $P(\sqrt{E_{\mathcal{R}}}x_{\mathcal{R}} = -a|T_2) = 1 - \sum_{k \in \{a, \pm b\}} P(\sqrt{E_{\mathcal{R}}}x_{\mathcal{R}} = k|T_2)$. We can obtain the probabilities for the other five cases by following the similar method.

Then we consider the conditional error probabilities, $P(\mathcal{E}|k, T_i)$, at the destination. we establish an *instantaneous destination constellation* (IDC) with X-axis being y_1 and Y-axis being y_2 based on the minimum Euclidean distance detection, as shown in Fig. 2. When the relay detects the received signal successfully and forwards the correct symbol, we define four reference points as

$$\begin{aligned}
V_1^{\mathcal{D}} &= (\sqrt{E_1}|h_{1\mathcal{D}}| + \sqrt{E_2}|h_{2\mathcal{D}}|, a|h_{\mathcal{R}\mathcal{D}}|), \quad V_2^{\mathcal{D}} = (-\sqrt{E_1}|h_{1\mathcal{D}}| + \sqrt{E_2}|h_{2\mathcal{D}}|, b|h_{\mathcal{R}\mathcal{D}}|), \\
V_3^{\mathcal{D}} &= (\sqrt{E_1}|h_{1\mathcal{D}}| - \sqrt{E_2}|h_{2\mathcal{D}}|, -b|h_{\mathcal{R}\mathcal{D}}|), \quad V_4^{\mathcal{D}} = (-\sqrt{E_1}|h_{1\mathcal{D}}| - \sqrt{E_2}|h_{2\mathcal{D}}|, -a|h_{\mathcal{R}\mathcal{D}}|).
\end{aligned} \tag{11}$$

Similar to IRC, the decision regions of IDC are segmented by the perpendicular bisectors of each edge in parallelogram according to Voronoi rule [21]. In particular, rays $l_{12}^{\mathcal{D}}$, $l_{13}^{\mathcal{D}}$, $l_{24}^{\mathcal{D}}$ and $l_{34}^{\mathcal{D}}$

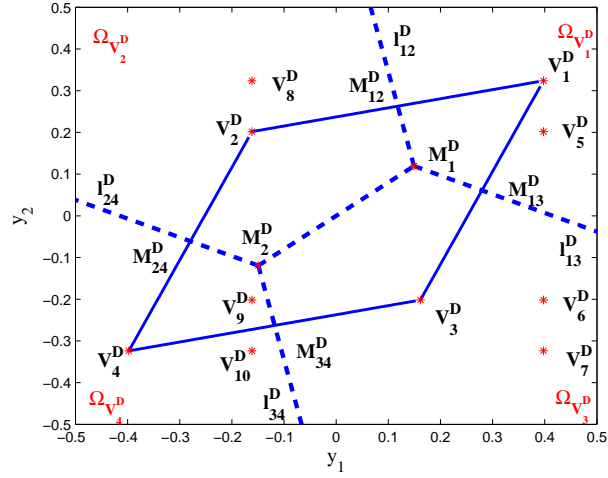


Fig. 2: Instantaneous destination constellation for network coded power adaption scheme. In particular, dashed lines represent boundaries of decision regions $\Omega_{V_i^D}$.

are perpendicular bisectors of sides $V_1^D V_2^D$, $V_1^D V_3^D$, $V_2^D V_4^D$ and $V_3^D V_4^D$, respectively. M_1^D is the crossing points of ray l_{12}^D and l_{13}^D , and M_2^D is the crossing points of ray l_{24}^D and l_{34}^D . Line segment $\overline{M_1^D M_2^D}$ is the perpendicular bisector of diagonal $\overline{V_2^D V_3^D}$. Then the correct decision region V_1^D at destination is

$$\Omega_{V_1^D} \triangleq \left\{ \frac{2\sqrt{E_1}|h_{1D}|}{(a-b)|h_{RD}|}y_1 + y_2 + M_1^D > 0 \cap \frac{2\sqrt{E_2}|h_{2D}|}{(a+b)|h_{RD}|}y_1 + y_2 + M_2^D > 0 \right\}, \quad (12)$$

where $M_1^D = -\frac{1}{2}(a+b)|h_{RD}| - 2\sqrt{E_1 E_2}|h_{1D}||h_{2D}||h_{RD}|$ and $M_2^D = -\frac{1}{2}(a-b)|h_{RD}| - 2\sqrt{E_1 E_2}|h_{1D}||h_{2D}||h_{RD}|$. Likewise, we can obtain $\Omega_{V_i^D}$ for $i = 2, 3, 4$.

When T_1 and T_2 are transmitted by the sources, the error probabilities at the destination given that relay transmits the correct symbol is denoted by $P(\mathcal{E}|\sqrt{E_{\mathcal{R}}}x_{\mathcal{R}} = a, T_1)$ and $P(\mathcal{E}|\sqrt{E_{\mathcal{R}}}x_{\mathcal{R}} = b, T_2)$, respectively. Let d_{ik}^D be the normalized distance between V_i^D and M_k^D in Fig. 2, which is given by $d_{ik}^D = \frac{|V_i^D - M_k^D|^2}{\sigma^2}$. Regarding the probability $P(\mathcal{E}|\sqrt{E_{\mathcal{R}}}x_{\mathcal{R}} = a, T_1)$, we have

$$P(\mathcal{E}|\sqrt{E_{\mathcal{R}}}x_{\mathcal{R}} = a, T_1) = 1 - P_{w_4}(d_{11}^D, \phi_1, \phi_2). \quad (13)$$

Defining \mathcal{P}^D as the region of parallelogram in IDC, the determinations of ϕ_1, ϕ_2 in (13) are as follows. When $\overline{V_1^D V_2^D} < \overline{V_1^D V_3^D}$ and $M_1^D, M_2^D \in \mathcal{P}^D$, we have $\phi_1 = \pi - \arcsin\left(\frac{\overline{V_1^D M_{13}^D}}{\overline{V_1^D M_1^D}}\right)$, $\phi_2 = \arcsin\left(\frac{\overline{V_1^D M_{12}^D}}{\overline{V_1^D M_1^D}}\right)$; When $\overline{V_1^D V_2^D} \geq \overline{V_1^D V_3^D}$ and $M_1^D, M_2^D \notin \mathcal{P}^D$, we have $\phi_1 = \arcsin\left(\frac{\overline{V_1^D M_{13}^D}}{\overline{V_1^D M_1^D}}\right)$, $\phi_2 = \pi - \arcsin\left(\frac{\overline{V_1^D M_{12}^D}}{\overline{V_1^D M_1^D}}\right)$; When $\overline{V_1^D V_2^D} \geq \overline{V_1^D V_3^D}$ and $M_1^D, M_2^D \in \mathcal{P}^D$, we have $\phi_1 = \arcsin\left(\frac{\overline{V_1^D M_{13}^D}}{\overline{V_1^D M_1^D}}\right)$, $\phi_2 = \arcsin\left(\frac{\overline{V_1^D M_{12}^D}}{\overline{V_1^D M_1^D}}\right)$.

Regarding the probability $P(\mathcal{E}|\sqrt{E_{\mathcal{R}}}x_{\mathcal{R}} = b, T_2)$, we have

$$P(\mathcal{E}|\sqrt{E_{\mathcal{R}}}x_{\mathcal{R}} = b, T_2) = 1 - P_{w_3}(d_{21}^{\mathcal{D}}, d_{22}^{\mathcal{D}}, \phi_1, \phi_2, \phi_3, \phi_4), \quad (14)$$

where $\phi_3 = \angle M_1^{\mathcal{D}} V_2^{\mathcal{D}} M_2^{\mathcal{D}}$ and $\phi_4 = \angle V_2^{\mathcal{D}} M_1^{\mathcal{D}} M_2^{\mathcal{D}}$. Further, the determinations of ϕ_1, ϕ_2 in (14) are as follows. When $\overline{V_1^{\mathcal{D}} V_2^{\mathcal{D}}} < \overline{V_1^{\mathcal{D}} V_3^{\mathcal{D}}}$ and $M_1^{\mathcal{D}}, M_2^{\mathcal{D}} \in \mathcal{P}^{\mathcal{D}}$, we have $\phi_1 = \arcsin\left(\frac{\overline{V_2^{\mathcal{D}} M_{12}^{\mathcal{D}}}}{\overline{V_2^{\mathcal{D}} M_1^{\mathcal{D}}}}\right)$ and $\phi_2 = \pi - \arcsin\left(\frac{\overline{V_2^{\mathcal{D}} M_{24}^{\mathcal{D}}}}{\overline{V_2^{\mathcal{D}} M_2^{\mathcal{D}}}}\right)$. Otherwise, we have $\phi_1 = \arcsin\left(\frac{\overline{V_2^{\mathcal{D}} M_{12}^{\mathcal{D}}}}{\overline{V_2^{\mathcal{D}} M_1^{\mathcal{D}}}}\right)$ and $\phi_2 = \arcsin\left(\frac{\overline{V_2^{\mathcal{D}} M_{24}^{\mathcal{D}}}}{\overline{V_2^{\mathcal{D}} M_2^{\mathcal{D}}}}\right)$.

When the relay detects the received signal unsuccessfully, the reference points in Eq. (11) will change according to the incorrect relay decisions. In particular, if sources transmit T_1 and the relay wrongly forwards $b, -b, a$, then the reference point $V_1^{\mathcal{D}}$ in Fig. 2 will change to $V_5^{\mathcal{D}}, V_6^{\mathcal{D}}$, and $V_7^{\mathcal{D}}$, respectively; If sources transmit T_2 and the relay wrongly forwards $a, -b, -a$, then the reference point $V_2^{\mathcal{D}}$ in Fig. 2 will change to $V_8^{\mathcal{D}}, V_9^{\mathcal{D}}$, and $V_{10}^{\mathcal{D}}$, respectively.

In the case when T_1 is transmitted by the sources, and the relay wrongly forwards $b, -b, a$, the error probabilities that destination makes wrong decisions are given by

$$P(\mathcal{E}|\sqrt{E_{\mathcal{R}}}x_{\mathcal{R}} = k_1, T_1) = \begin{cases} 1 - P_{w_4}(d_{j1}^{\mathcal{D}}, \phi_1, \phi_2), & \text{when } V_j^{\mathcal{D}} \in \Omega_{V_1^{\mathcal{D}}}, \\ 1 - P_{w_1}(d_{j1}^{\mathcal{D}}, \phi_1, \phi_2), & \text{when } V_j^{\mathcal{D}} \notin \Omega_{V_1^{\mathcal{D}}}, \end{cases} \quad (15)$$

where when $k_1 = b, -b, a$, then $j = 5, 6, 7$, respectively.

In the case when T_2 is transmitted by the sources, and the relay wrongly forwards $a, -b, -a$, the error probabilities that destination makes wrong decisions are given by

$$P(\mathcal{E}|\sqrt{E_{\mathcal{R}}}x_{\mathcal{R}} = k_2, T_2) = \begin{cases} 1 - P_{w_3}(d_{l1}^{\mathcal{D}}, d_{l2}^{\mathcal{D}}, \phi_1, \phi_2, \phi_3, \phi_4, 1, 1), & \text{when } V_l^{\mathcal{D}} \in \Omega_{V_2^{\mathcal{D}}}, \\ 1 - P_{w_3}(d_{l2}^{\mathcal{D}}, d_{l1}^{\mathcal{D}}, \phi_1, \phi_2, \phi_3, \phi_4, 1, 1), & \text{when } V_l^{\mathcal{D}} \notin \Omega_{V_2^{\mathcal{D}}}, \end{cases} \quad (16)$$

where when $k_1 = a, -b, -a$, then $l = 8, 9, 10$, respectively. Note that the determinations on the related angles ϕ_1, ϕ_2, ϕ_3 , and ϕ_4 are shown in Table I and Table II.

TABLE I: Correspondence Parameters of $P(\mathcal{E}|\sqrt{E_{\mathcal{R}}}x_{\mathcal{R}} = k_1, T_1)$

$V_j^{\mathcal{D}} \in \Omega_{V_1^{\mathcal{D}}}$			$V_j^{\mathcal{D}} \notin \Omega_{V_1^{\mathcal{D}}}$		
$M_1, M_2 \notin \mathcal{P}^{\mathcal{D}}$		$M_1, M_2 \in \mathcal{P}^{\mathcal{D}}$	$M_1, M_2 \notin \mathcal{P}^{\mathcal{D}}$		$M_1, M_2 \in \mathcal{P}^{\mathcal{D}}$
$\overline{V_1^{\mathcal{D}} V_2^{\mathcal{D}}} < \overline{V_1^{\mathcal{D}} V_3^{\mathcal{D}}}$	$\overline{V_1^{\mathcal{D}} V_2^{\mathcal{D}}} \geq \overline{V_1^{\mathcal{D}} V_3^{\mathcal{D}}}$	-	$\overline{V_1^{\mathcal{D}} V_2^{\mathcal{D}}} < \overline{V_1^{\mathcal{D}} V_3^{\mathcal{D}}}$	$\overline{V_1^{\mathcal{D}} V_2^{\mathcal{D}}} \geq \overline{V_1^{\mathcal{D}} V_3^{\mathcal{D}}}$	-
$\phi_1 = \angle V_j^{\mathcal{D}} M_1^{\mathcal{D}} M_{12}^{\mathcal{D}}$	$\phi_1 = \pi - \angle V_j^{\mathcal{D}} M_1^{\mathcal{D}} M_{12}^{\mathcal{D}}$	$\phi_1 = \angle V_j^{\mathcal{D}} M_1^{\mathcal{D}} M_{12}^{\mathcal{D}}$	$\phi_1 = \pi - \angle V_j^{\mathcal{D}} M_1^{\mathcal{D}} M_{12}^{\mathcal{D}}$	$\phi_1 = \angle V_j^{\mathcal{D}} M_1^{\mathcal{D}} M_{13}^{\mathcal{D}}$	$\phi_1 = \angle V_j^{\mathcal{D}} M_1^{\mathcal{D}} M_{12}^{\mathcal{D}}$
$\phi_2 = \pi - \angle V_j^{\mathcal{D}} M_1^{\mathcal{D}} M_{13}^{\mathcal{D}}$	$\phi_2 = \angle V_j^{\mathcal{D}} M_1^{\mathcal{D}} M_{13}^{\mathcal{D}}$	$\phi_2 = \angle V_j^{\mathcal{D}} M_1^{\mathcal{D}} M_{13}^{\mathcal{D}}$	$\phi_2 = \angle V_j^{\mathcal{D}} M_1^{\mathcal{D}} M_{13}^{\mathcal{D}}$	$\phi_2 = \pi - \angle V_j^{\mathcal{D}} M_1^{\mathcal{D}} M_{12}^{\mathcal{D}}$	$\phi_2 = \pi - \angle V_j^{\mathcal{D}} M_1^{\mathcal{D}} M_{13}^{\mathcal{D}}$

B. SPER Based on Coordinate Transformation

We observe that the SPER based on wedge probabilities is diversified into several cases due to varying channel coefficients. Although the SPER result is accurate by using the wedge

TABLE II: Correspondence Parameters of $P(\mathcal{E}|\sqrt{E_{\mathcal{R}}}x_{\mathcal{R}} = k_2, T_2)$

$V_l^{\mathcal{D}} \in \Omega_{V_2^{\mathcal{D}}}$	$V_l^{\mathcal{D}} \notin \Omega_{V_2^{\mathcal{D}}}$			
-	$V_l^{\mathcal{D}}$ is above line $M_1^{\mathcal{D}}M_2^{\mathcal{D}}$		$V_l^{\mathcal{D}}$ is below line $M_1^{\mathcal{D}}M_2^{\mathcal{D}}$	
-	$M_1^{\mathcal{D}}, M_2^{\mathcal{D}} \notin \mathcal{P}^{\mathcal{D}}$	$M_1^{\mathcal{D}}, M_2^{\mathcal{D}} \in \mathcal{P}^{\mathcal{D}}$	$M_1^{\mathcal{D}}, M_2^{\mathcal{D}} \notin \mathcal{P}^{\mathcal{D}}$	$M_1^{\mathcal{D}}, M_2^{\mathcal{D}} \in \mathcal{P}^{\mathcal{D}}$
$\phi_1 = \angle V_l^{\mathcal{D}} M_1^{\mathcal{D}} M_{12}^{\mathcal{D}}$	$\phi_1 = \angle V_l^{\mathcal{D}} M_1^{\mathcal{D}} M_2^{\mathcal{D}}$	$\phi_1 = \pi - \angle V_l^{\mathcal{D}} M_2^{\mathcal{D}} M_1^{\mathcal{D}}$	$\phi_1 = \pi - \angle V_l^{\mathcal{D}} M_2^{\mathcal{D}} M_{24}^{\mathcal{D}}$	$\phi_1 = \pi - \angle V_l^{\mathcal{D}} M_1^{\mathcal{D}} M_{12}^{\mathcal{D}}$
$\phi_2 = \angle V_l^{\mathcal{D}} M_2^{\mathcal{D}} M_{24}^{\mathcal{D}}$	$\phi_2 = \pi - \angle V_l^{\mathcal{D}} M_1^{\mathcal{D}} M_{12}^{\mathcal{D}}$	$\phi_2 = \pi - \angle V_l^{\mathcal{D}} M_2^{\mathcal{D}} M_{24}^{\mathcal{D}}$	$\phi_2 = \angle V_l^{\mathcal{D}} M_2^{\mathcal{D}} M_1^{\mathcal{D}}$	$\phi_2 = \pi - \angle V_l^{\mathcal{D}} M_1^{\mathcal{D}} M_2^{\mathcal{D}}$
$\phi_3 = \angle V_l^{\mathcal{D}} M_1^{\mathcal{D}} M_2^{\mathcal{D}}$	$\phi_3 = \pi - \angle V_l^{\mathcal{D}} M_2^{\mathcal{D}} M_1^{\mathcal{D}}$	$\phi_3 = \angle V_l^{\mathcal{D}} M_1^{\mathcal{D}} M_2^{\mathcal{D}}$	$\phi_3 = \pi - \angle V_l^{\mathcal{D}} M_1^{\mathcal{D}} M_{12}^{\mathcal{D}}$	$\phi_3 = \angle V_l^{\mathcal{D}} M_2^{\mathcal{D}} M_{24}^{\mathcal{D}}$
$\phi_4 = \angle M_1^{\mathcal{D}} V_l^{\mathcal{D}} M_2^{\mathcal{D}}$	$\phi_4 = \pi - \angle V_l^{\mathcal{D}} M_2^{\mathcal{D}} M_{24}^{\mathcal{D}}$	$\phi_4 = \pi - \angle V_l^{\mathcal{D}} M_1^{\mathcal{D}} M_{12}^{\mathcal{D}}$	$\phi_4 = \pi - \angle V_l^{\mathcal{D}} M_1^{\mathcal{D}} M_2^{\mathcal{D}}$	$\phi_4 = \angle V_l^{\mathcal{D}} M_2^{\mathcal{D}} M_1^{\mathcal{D}}$

probability method, the calculations of the SPER could be very complicated. Here, we will propose a coordinate transformation method to derive the SPER, which reduces the calculation complexity by sacrificing a little accuracy in the low SNR region. Specifically, our coordinate transformation method transforms the original parallelogram geometry in the wedge potability method to a rectangle geometry, based on which, we determine the decision regions of the new constellations. The following lemma derives the coordinate transformation matrix at relay node.

Lemma 1: The coordinate transformation matrix \mathbf{C} , which transforms the exact parallelogram-shaped IRC to a rectangle centered at origin point, and preserve the length of each side in exact IRC is given by

$$\mathbf{C} = \mathbf{Q}\mathbf{A}^{-1}, \quad (17)$$

where \mathbf{Q} is the eigenvector matrix for $\mathbf{B} = \mathbf{A}^T \Sigma^{-1} \mathbf{A}$ given in (43), shown as

$$\mathbf{Q} = \begin{bmatrix} \frac{\mathbf{B}(1,2)}{(\lambda_1 - \lambda_2) \sqrt{\frac{\mathbf{B}(1,1) - \lambda_1}{\lambda_2 - \lambda_1}}} & \sqrt{\frac{\mathbf{B}(1,1) - \lambda_1}{\lambda_2 - \lambda_1}} \\ \sqrt{\frac{\mathbf{B}(1,1) - \lambda_1}{\lambda_2 - \lambda_1}} & -\frac{\mathbf{B}(1,2)}{(\lambda_1 - \lambda_2) \sqrt{\frac{\mathbf{B}(1,1) - \lambda_1}{\lambda_2 - \lambda_1}}} \end{bmatrix}, \text{ and } \mathbf{A}^{-1} = \begin{bmatrix} \frac{\Re\{h_{1\mathcal{R}}\}}{2|h_{1\mathcal{R}}|} & \frac{\Re\{h_{2\mathcal{R}}\}}{2|h_{2\mathcal{R}}|} \\ \frac{\Im\{h_{1\mathcal{R}}\}}{2|h_{1\mathcal{R}}|} & \frac{\Im\{h_{2\mathcal{R}}\}}{2|h_{2\mathcal{R}}|} \end{bmatrix}. \quad (18)$$

where the eigenvalues λ_1 and λ_2 are derived in (44).

Proof: The proof of Lemma 1 is illustrated in Appendix B. ■

Now, we will determine the decision regions of the new IRC. Denote $\bar{\mathbf{V}}_i$ the constellation point and $\bar{\mathbf{Z}}$ the received signal point ($\Re\{y_{\mathcal{R}}\}, \Im\{y_{\mathcal{R}}\}$) after coordinate transformation by matrix \mathbf{B} , respectively. Denote $\bar{\Omega}_{\bar{\mathbf{V}}_i}$ the decision region corresponding to $\bar{\mathbf{V}}_i$. The boundary is defined based on Voronoi rule

$$\begin{aligned} \bar{\Omega}_{\bar{\mathbf{V}}_1} : \Re\{\bar{\mathbf{Z}}\} - \Im\{\bar{\mathbf{Z}}\} > 0 \cap \Re\{\bar{\mathbf{Z}}\} + \Im\{\bar{\mathbf{Z}}\} \leq 0, \quad \bar{\Omega}_{\bar{\mathbf{V}}_2} : \Re\{\bar{\mathbf{Z}}\} - \Im\{\bar{\mathbf{Z}}\} > 0 \cap \Re\{\bar{\mathbf{Z}}\} + \Im\{\bar{\mathbf{Z}}\} > 0, \\ \bar{\Omega}_{\bar{\mathbf{V}}_3} : \Re\{\bar{\mathbf{Z}}\} - \Im\{\bar{\mathbf{Z}}\} \leq 0 \cap \Re\{\bar{\mathbf{Z}}\} + \Im\{\bar{\mathbf{Z}}\} > 0, \quad \bar{\Omega}_{\bar{\mathbf{V}}_4} : \Re\{\bar{\mathbf{Z}}\} - \Im\{\bar{\mathbf{Z}}\} \leq 0 \cap \Re\{\bar{\mathbf{Z}}\} + \Im\{\bar{\mathbf{Z}}\} \leq 0. \end{aligned} \quad (19)$$

In Fig. 3, we present the constellation after coordinate transformation and its decision regions.

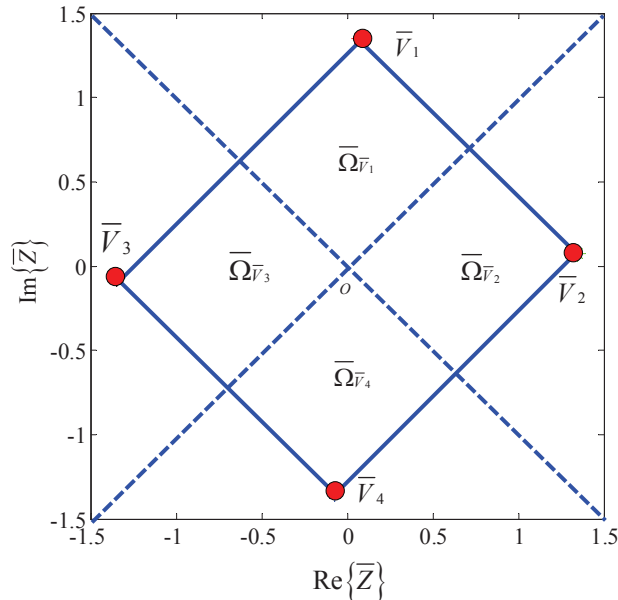


Fig. 3: Received Constellation at Relay after Coordinate Transformation.

From (19), we can see that the decision regions are regular geometry with simple decision boundary lines². Thus, it will greatly reduce the computational complexity. The probabilities that relay detects the received signal when T_1 is sent are shown as

$$P(\sqrt{E_{\mathcal{R}}}x_{\mathcal{R}} = a|T_1) = \int_0^{\infty} d(\Im\{\bar{Z}\}) \int_{-\Im\{\bar{Z}\}}^{\Im\{\bar{Z}\}} f_{\bar{Z}}(\bar{Z}; \Re\{\bar{\mathbf{V}}_i\}, \Im\{\bar{\mathbf{V}}_i\}) d(\Re\{\bar{Z}\}), \quad (20)$$

where $f_{\bar{Z}}(\cdot)$ is the probability density function of \bar{Z} given in (40), $\bar{\mathbf{V}}_i(1)$ and $\bar{\mathbf{V}}_i(2)$ represent the horizontal coordinate and vertical coordinate of $\bar{\mathbf{V}}_i$, respectively. Similar to (20), we can obtain $P(\sqrt{E_{\mathcal{R}}}x_{\mathcal{R}} = k|T_1)$ for $k \in \{\pm b, -a\}$ and the probabilities that relay detects the received signal when T_2 is sent.

Similar to the error probability analysis at relay, we will show the results of coordinate transformation and the error probability based on the new constellation at destination. In the following lemma, we present the coordinate transformation matrix $\mathbf{C}_{\mathcal{D}}$ at destination.

Lemma 2: At destination, the coordinate transformation matrix $\mathbf{C}_{\mathcal{D}}$, which transform the exact IDC to a rectangle centered at origin point, and preserve the length of each side in exact

²Note that the real decision boundary lines are slightly different from the perpendicular bisectors of Voronoi diagram after coordinate transformation. This is why the SPER results of coordinate transformation have notably little difference in low SNR comparing with its counterpart of exact constellation. As the SNR goes larger, the real decision boundary lines are coincide with the perpendicular bisectors.

parallelogram-shaped IDC is given by

$$\mathbf{C}_D = \mathbf{Q}_D \mathbf{A}_D^{-1}, \quad (21)$$

where \mathbf{Q}_D is the eigenvector matrix for \mathbf{B}_D shown as

$$\mathbf{B}_D = \frac{2}{\beta_D^2 \sigma^2} \begin{bmatrix} d_1^2(a+b)^2|h_{\mathcal{RD}}|^2 + 4d_1^2|h_{2D}|^2 & d_1d_2(b^2-a^2)|h_{\mathcal{RD}}|^2 - 4d_1d_2|h_{1D}||h_{2D}| \\ d_1d_2(b^2-a^2)|h_{\mathcal{RD}}|^2 - 4d_1d_2|h_{1D}||h_{2D}| & d_2^2(b-a)^2|h_{\mathcal{RD}}|^2 + 4d_2^2|h_{2D}|^2 \end{bmatrix}, \quad (22)$$

where $\beta_D = h_{\mathcal{RD}}(|h_{1D}|(a+b) + |h_{2D}|(b-a))$, $d_1 = \sqrt{4|h_{1D}|^2 + (a-b)^2|h_{\mathcal{RD}}|^2}$ and $d_2 = \sqrt{4|h_{2D}|^2 + (a+b)^2|h_{\mathcal{RD}}|^2}$. And

$$\mathbf{Q}_D = \begin{bmatrix} \frac{\mathbf{B}_D(1,2)}{(\lambda_1^D - \lambda_2^D) \sqrt{\frac{\mathbf{B}_D(1,1) - \lambda_1^D}{\lambda_2^D - \lambda_1^D}}} & \sqrt{\frac{\mathbf{B}_D(1,1) - \lambda_1^D}{\lambda_2^D - \lambda_1^D}} \\ \sqrt{\frac{\mathbf{B}_D(1,1) - \lambda_1^D}{\lambda_2^D - \lambda_1^D}} & -\frac{\mathbf{B}_D(1,2)}{(\lambda_1^D - \lambda_2^D) \sqrt{\frac{\mathbf{B}_D(1,1) - \lambda_1^D}{\lambda_2^D - \lambda_1^D}}} \end{bmatrix}, \text{ and } \mathbf{A}_D^{-1} = \begin{bmatrix} (a+b)|h_{\mathcal{RD}}| & -|h_{2D}| \\ (a-b)|h_{\mathcal{RD}}| & -|h_{1D}| \end{bmatrix}. \quad (23)$$

where the eigenvalues λ_1^D and λ_2^D are eigenvalues of \mathbf{B}_D .

Lemma 2 can be obtained in the same way as we formulated at relay. Now, we will determine the decision regions with the new IDC. Denote $\bar{\mathbf{V}}_i^D$ the constellation point and \bar{Z}_D the received signal after coordinate transformation by matrix \mathbf{C}_D . Denote $\bar{\Omega}_{\bar{\mathbf{V}}_i^D}^D$ the decision region corresponding to $\bar{\mathbf{V}}_i^D$. The boundary is defined based on Voronoi rule

$$\bar{\Omega}_{\bar{\mathbf{V}}_1^D}^D : \bar{Z}_D(1) - \bar{Z}_D(2) > 0 \cap \bar{Z}_D(1) + \bar{Z}_D(2) \leq 0, \quad \bar{\Omega}_{\bar{\mathbf{V}}_2^D}^D : \bar{Z}_D(1) - \bar{Z}_D(2) > 0 \cap \bar{Z}_D(1) + \bar{Z}_D(2) > 0, \quad (24)$$

$$\bar{\Omega}_{\bar{\mathbf{V}}_3^D}^D : \bar{Z}_D(1) - \bar{Z}_D(2) \leq 0 \cap \bar{Z}_D(1) + \bar{Z}_D(2) > 0, \quad \bar{\Omega}_{\bar{\mathbf{V}}_4^D}^D : \bar{Z}_D(1) - \bar{Z}_D(2) \leq 0 \cap \bar{Z}_D(1) + \bar{Z}_D(2) \leq 0,$$

where $\bar{Z}_D(1)$ and $\bar{Z}_D(2)$ represent the horizontal coordinate and vertical coordinate of \bar{Z}_D , respectively.

Based on the decision regions of new IDC, the probability that destination detects the received signal successfully and unsuccessfully when T_1 is sent are shown respectively as

$$P\left(\mathcal{E} | \sqrt{E_{\mathcal{R}}} x_{\mathcal{R}} = a, T_1\right) = \int_0^\infty d(\bar{Z}_D(2)) \int_{-\bar{Z}_D(2)}^{\bar{Z}_D(2)} f_{\bar{Z}_D}\left(\bar{Z}_D; \bar{\mathbf{V}}_i^D(1), \bar{\mathbf{V}}_i^D(2)\right) d(\bar{Z}_D(1)), \quad (25)$$

where $f_{\bar{Z}_D}(\cdot)$ is the probability density function of \bar{Z}_D , $\bar{\mathbf{V}}_i^D(1)$ and $\bar{\mathbf{V}}_i^D(2)$ represent the horizontal coordinate and vertical coordinate of $\bar{\mathbf{V}}_i^D$, respectively. Similar to (25), we can obtain $P(\mathcal{E} | \sqrt{E_{\mathcal{R}}} x_{\mathcal{R}} = k, T_1)$ for $k \in \{\pm b, -a\}$ and the probabilities that relay detects the received signal when T_2 is sent.

Based on (20) and (25), we can calculate the SPER shown in (8) based on the constellation after coordinate transformation.

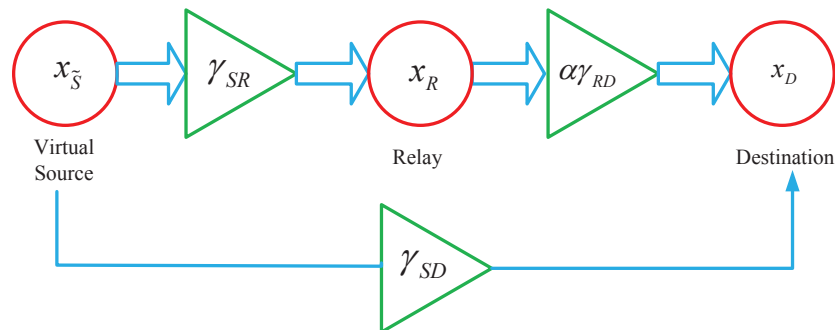


Fig. 4: Virtual channel model.

V. SYSTEM OPTIMIZATION

In this section, we first develop a practical method at the relay side to address the error propagation problem. With the designed method, the system is proved to achieve full diversity when the relay implements non-perfect detection. Specifically, we propose a power scaling scheme where the relay power is adaptive to the channel conditions. For such link adaptive relaying (LAR) scheme, we model the complicated MARC system as a degraded virtual one-source one-relay one destination model (triangle model), and show that the relay power should be such to balance the SNRs of source-relay channel and relay-destination channel. Moreover, we formulate a sub-optimal Max-min method to obtain the optimized system parameters a and b that minimize the end-to-end SER.

A. The Design of Power Scaling Factor at Relay

Before introducing the design of power scaling factor at relay, we would present the diversity performance of the proposed PANC scheme and the CXNC scheme in the following Proposition.

Theorem 1: Without the design of power scaling factor at relay, both the PANC scheme and the CXNC scheme can only achieve one order diversity in the MARC system.

Proof: Please refer to Appendix C.

From Theorem 1, we can see that the error propagation from the early source-relay hop degrades the performance of the system. In this case, we adopt a power scaling factor at relay to leverage the effect of error propagation by adjusting the relay transmission power according to the channel conditions. Such link adaptive ratio (LAR) was first introduced for the single-source DF system in [23]. However, LAR cannot be directly applied to the multi-user power adapted network coding system.

To extend the spirit of LAR, we first develop a virtual channel model for the source-relay-destination link, as shown in Fig. 4. In the first phase, the two sources transmit to relay simultaneously. For such multiple-access channel, the upper bound for the instantaneous SER is given by

$$P_{\text{MAC}} \leq P_{\text{MAC}}^U \triangleq Q_1 \left(\sqrt{2E_1|h_{1\mathcal{R}}|^2/\sigma^2} \right) + Q_1 \left(\sqrt{2E_2|h_{2\mathcal{R}}|^2/\sigma^2} \right) + Q_1 \left(\sqrt{2|\sqrt{E_1}h_{1\mathcal{R}} + \sqrt{E_2}h_{2\mathcal{R}}|^2/\sigma^2} \right), \quad (26)$$

which can be further approximated as

$$P_{\text{MAC}}^U \approx Q_1 \left(\sqrt{2 \min \left[E_1|h_{1\mathcal{R}}|^2/\sigma^2, E_2|h_{2\mathcal{R}}|^2/\sigma^2, |\sqrt{E_1}h_{1\mathcal{R}} + \sqrt{E_2}h_{2\mathcal{R}}|^2/\sigma^2 \right]} \right), \quad (27)$$

which is quite tight when $E_1|h_{1\mathcal{R}}|^2/\sigma^2$, $E_2|h_{2\mathcal{R}}|^2/\sigma^2$, $|\sqrt{E_1}h_{1\mathcal{R}} + \sqrt{E_2}h_{2\mathcal{R}}|^2/\sigma^2$ and their difference are reasonably large, as the one-dimensional Q-function $Q_1(x)$ decays fast as x grows. The advantage of such approximation is that we can now model the multiple access source-relay channel as a single-input single-output channel with the input being the virtual source message $x_{\tilde{s}} = x_1 \boxplus x_2$ and the instantaneous channel SNR being $\gamma_{S\mathcal{R}} \triangleq \min(E_1|h_{1\mathcal{R}}|^2, E_2|h_{2\mathcal{R}}|^2, |\sqrt{E_1}h_{1\mathcal{R}} + \sqrt{E_2}h_{2\mathcal{R}}|^2)$ that is the SNR of the worse source-relay channel³. The idea of regarding virtual source message as network coded sources' signals is that we implement network coding at relay node. Thus, the virtual transmitting information from source to destination via the aid of relay becomes the same. Likely, we can model the multiple access source-destination channel as a point-to-point channel with the channel SNR as γ_{SD} . So far, we have successfully degrade the complex MARC system to a traditional triangle model. Based on the conclusion in [23], the power scaling factor α with instantaneous $\gamma_{S\mathcal{R}}$ and $\gamma_{\mathcal{R}\mathcal{D}}$ is given by

$$\alpha = \min \left(\frac{\gamma_{S\mathcal{R}}}{\gamma_{\mathcal{R}\mathcal{D}}}, 1 \right). \quad (28)$$

Note that, instantaneous channel SNR $\gamma_{\mathcal{R}\mathcal{D}}$ can be replaced by statistical channel SNR $\bar{\gamma}_{\mathcal{R}\mathcal{D}}$. The advantage of using $\bar{\gamma}_{\mathcal{R}\mathcal{D}}$ to obtain α is that the relay node does not need the feedback of relay-destination channel. Later, we will show that both instantaneous and statistical relay-destination channel SNR can achieve full diversity in the proposed PANC scheme.

Theorem 2: Given instantaneous source-relay channel SNR, and instantaneous (or statistical) relay-destination channel SNR, the power scaled PANC scheme can achieve two order diversity,

³Note that our approximation is different from the one shown in [16], in which the authors consider an orthogonal MARC system.

i.e., the full diversity, in the MARC system, while the power scaled conventional NC scheme can only achieve one order diversity.

Proof: Please refer to Appendix D.

B. The Design of Power Adaption Factors

From the derivations of the instantaneous system SPER in Section IV, we note that the expressions of the SPER depends on the power adaption levels a and b at the relay. To minimize the SPER requires a smart optimization on a and b . However, directly minimizing the SPER is very complicated and leads to no closed forms of a and b . Here, we propose a sub-optimal criterion for the instantaneous SPER minimization, i.e., maximizing the minimum Euclidean distances of the instantaneous constellation at the destination. The *Max-min* optimization problem under the power constraint is formulated as

$$\begin{aligned} (a^*, b^*) &= \arg \max_{a,b} \min_{k,j=1,2,3,4;k \neq j} \{ \|V_k^{\mathcal{D}} - V_j^{\mathcal{D}}\|^2 \} \\ \text{s. t. } &a^2 + b^2 \leq 2E_{\mathcal{R}}^{\text{ave}}, \quad a, b \in \mathbb{R}, \end{aligned} \quad (29)$$

where the lengths of parallelogram's two edges are $\overrightarrow{V_1^{\mathcal{D}}V_2^{\mathcal{D}}} = \|V_1^{\mathcal{D}} - V_2^{\mathcal{D}}\|^2 = 4E_1|h_{1\mathcal{D}}|^2 + |h_{\mathcal{R}\mathcal{D}}|^2(a-b)^2$ and $\overrightarrow{V_1^{\mathcal{D}}V_3^{\mathcal{D}}} = 4E_2|h_{2\mathcal{D}}|^2 + |h_{\mathcal{R}\mathcal{D}}|^2(a+b)^2$, and the lengths of diagonals are $\overrightarrow{V_2^{\mathcal{D}}V_3^{\mathcal{D}}} = (-2\sqrt{E_1}|h_{1\mathcal{D}}| + 2\sqrt{E_2}|h_{2\mathcal{D}}|)^2 + 4|h_{\mathcal{R}\mathcal{D}}|^2b^2$ and $\overrightarrow{V_1^{\mathcal{D}}V_4^{\mathcal{D}}} = (2\sqrt{E_1}|h_{1\mathcal{D}}| + 2\sqrt{E_2}|h_{2\mathcal{D}}|)^2 + 4|h_{\mathcal{R}\mathcal{D}}|^2a^2$. Defining \mathcal{V} as the set of $\{\overrightarrow{V_1^{\mathcal{D}}V_2^{\mathcal{D}}}, \overrightarrow{V_1^{\mathcal{D}}V_3^{\mathcal{D}}}, \overrightarrow{V_2^{\mathcal{D}}V_3^{\mathcal{D}}}, \overrightarrow{V_1^{\mathcal{D}}V_4^{\mathcal{D}}}\}$, and introducing a variable $u \triangleq \min\{\mathcal{V}\}$, after some manipulations, the *Max-min* problem in (29) can be further described as a maximization problem

$$\begin{aligned} &\max_{(u^*, a^*, b^*)} u \\ \text{s. t. } &-(4E_1|h_{1\mathcal{D}}|^2 + |h_{\mathcal{R}\mathcal{D}}|^2(a-b)^2) \leq -u, \quad -(4E_2|h_{2\mathcal{D}}|^2 + |h_{\mathcal{R}\mathcal{D}}|^2(a+b)^2) \leq -u, \\ &-(c_1 + 4|h_{\mathcal{R}\mathcal{D}}|^2b^2) \leq -u, \quad -(c_2 + 4|h_{\mathcal{R}\mathcal{D}}|^2a^2) \leq -u, \quad a^2 + b^2 \leq 2E_{\mathcal{R}}^{\text{ave}}, \end{aligned} \quad (30)$$

where $c_1 = (-2\sqrt{E_1}|h_{1\mathcal{D}}| + 2\sqrt{E_2}|h_{2\mathcal{D}}|)^2$ and $c_2 = (2\sqrt{E_1}|h_{1\mathcal{D}}| + 2\sqrt{E_2}|h_{2\mathcal{D}}|)^2$. Since the objective function is an affine function and the constraints are quadratic functions of a and b in (30), it is a convex optimization problem. We can adopt the Lagrange Multiplier method to obtain the solutions. The Lagrange equation is given by

$$\begin{aligned} L(a, b, u, \mu_1, \mu_2, \mu_3, \mu_4, \mu_5) &= u + \mu_1(u - 4E_1|h_{1\mathcal{D}}|^2 - |h_{\mathcal{R}\mathcal{D}}|^2(a-b)^2) + \mu_2(u - 4E_2|h_{2\mathcal{D}}|^2 - |h_{\mathcal{R}\mathcal{D}}|^2(a+b)^2) \\ &+ \mu_3(u - c_1 - 4|h_{\mathcal{R}\mathcal{D}}|^2b^2) + \mu_4(u - c_2 - 4|h_{\mathcal{R}\mathcal{D}}|^2a^2) + \mu_5(a^2 + b^2 - E_{\mathcal{R}}^{\text{ave}}). \end{aligned} \quad (31)$$

After some intermediate manipulations, we obtain one of the optimal solutions for the problem in (30) in the case $\mu_1 = \mu_2 = 0, \mu_3 \neq 0, \mu_4 \neq 0$, and $\mu_5 \neq 0$ as follows.

$$(a^*, b^*) = \left(\sqrt{E_{\mathcal{R}}^{\text{ave}} + \frac{c_1 - c_2}{8|h_{\mathcal{RD}}|^2}}, \sqrt{E_{\mathcal{R}}^{\text{ave}} + \frac{c_2 - c_1}{8|h_{\mathcal{RD}}|^2}} \right). \quad (32)$$

Note that there are total 32 optimal solutions by adopting different $\mu_1, \mu_2, \mu_3, \mu_4$ and μ_5 , which can be obtained similarly by adopting the KKT conditions. But one of these solutions is sufficient to achieve the optimal u .

We can also formulate the *Max-min* method for the coordinate transformed IDC proposed in Subsection B of Section IV, which simplifies the calculations of the SPER. Here, based on the coordinate transformed IDC, we can also simplify the optimization process of a and b . Specifically in the *Max-min* problem described in (29), we only consider the the two edges of the rectangle in the coordinate transformed IDC, since the two edges are always less than the diagonals of the rectangle. Likewise, we can implement the *Max-min* method to obtain the optimal a and b based on the IDC after coordinated transforming, one of the solution is

$$\begin{aligned} a^* &= \frac{1}{2} \left(\sqrt{\frac{2(E_{\mathcal{R}}^{\text{ave}}|h_{\mathcal{RD}}|^2 + E_2|h_{2\mathcal{D}}|^2 - E_1|h_{1\mathcal{D}}|^2)}{|h_{\mathcal{RD}}|^2}} + \sqrt{\frac{2(E_{\mathcal{R}}^{\text{ave}}|h_{\mathcal{RD}}|^2 + E_1|h_{1\mathcal{D}}|^2 - E_2|h_{2\mathcal{D}}|^2)}{|h_{\mathcal{RD}}|^2}} \right), \\ b^* &= \frac{1}{2} \left(\sqrt{\frac{2(E_{\mathcal{R}}^{\text{ave}}|h_{\mathcal{RD}}|^2 + E_1|h_{1\mathcal{D}}|^2 - E_2|h_{2\mathcal{D}}|^2)}{|h_{\mathcal{RD}}|^2}} - \sqrt{\frac{2(E_{\mathcal{R}}^{\text{ave}}|h_{\mathcal{RD}}|^2 + E_2|h_{2\mathcal{D}}|^2 - E_1|h_{1\mathcal{D}}|^2)}{|h_{\mathcal{RD}}|^2}} \right). \end{aligned} \quad (33)$$

VI. SIMULATION RESULTS

In this section, we evaluate the performance of the proposed PANC scheme by simulations. Consider a two-dimensional cartesian coordinate system, where nodes $\mathcal{S}_1, \mathcal{S}_2$ and \mathcal{D} are located at $(0, \frac{\sqrt{3}}{3}), (0, -\frac{\sqrt{3}}{3}),$ and $(1, 0)$, respectively. The relay node is moving from origin point $(0, 0)$ to $(1, 0)$ at X-axis. Throughout our simulations, we use the path loss model $\gamma_{ij} = d_{ij}^{-3}$, where γ_{ij} is the channel gain and d_{ij} is the distance between two terminals, where $i \in \{\mathcal{S}_1, \mathcal{S}_2, \mathcal{R}\}$ and $j \in \{\mathcal{R}, \mathcal{D}\}$. The average SNR range is $[0, 30]$ dB. To simplify the expression in the legends of simulation results, 'sim' stands for Monte-Carlo simulation result, 'thy' stands for theoretical derivation result.

In order to investigate the performance of our proposed scheme comprehensively, we consider the relay located at different locations resulting in different channel scenarios. Firstly, we consider the relay is located at $(0, 0)$, so the relay is close to the sources, i.e., asymmetric network with

strong source-relay channel, shown in Fig. 5. Then, we consider the relay is located at $(\frac{1}{3}, 0)$, so the distance between source and relay is equal to the distance between relay and destination, i.e., a symmetric network, shown in Fig. 6. Finally, we consider the relay is located at $(0.8, 0)$, so the distance between sources and relay is larger than the distance between relay to destination, i.e., asymmetric network with strong relay-destination channel, shown in Fig. 7.

In each realization of nodes locations, we simulate the following schemes to demonstrate the performance of the proposed PANC scheme: (1) the SPER performance of original received constellation with optimized a and b given in (32), for both monte carlo simulation and theoretically derived result, denoted by *Origin-sim* and *Origin-thy*, respectively. (2) the SPER performance of received constellation after coordinate transformation with optimized a and b given in (33), for both monte carlo simulation and theoretically derived result, denoted by *CT-sim* and *CT-thy*, respectively.

As the references, we also simulate the following schemes: (1) the SPER performance of CXNC scheme [8], [9] in which the relay transmits XORed signal to the destination in the second transmission phase, denoted by *CXNC*; (2) The SPER performance of CXNC scheme in which the relay transmits power scaled XORed signal to the destination in the second transmission phase, denoted by *CXNC _{α}* ; (3) The SPER performance of genie-aided PANC scheme which is under the assumption that the symbols are perfectly detected at relay, denoted by *Genie*; (4) The SPER performance of PANC scheme with randomly generated a and b , in which a is a uniformly distributed random variable in $[0, \sqrt{2}]$ and $b = \sqrt{2E_{\mathcal{R}} - a^2}$, and both a and b vary in different instantaneous CSI, denoted by *Random*; (5) the SPER performance of PANC scheme with fixed chosen a and b , in which a is a uniformly distributed random variable in $[0, \sqrt{2}]$ and $b = \sqrt{2E_{\mathcal{R}} - a^2}$. Once both a and b are generated, they will remain the same for all CSI, denoted by *Fixed*.

Firstly, the CXNC without power scaling can only achieve one order diversity, since the error propagation from the early source-relay hop degrades the performance of the system as Theorem 1 indicates. The CXNC with power scaling cannot either achieve full diversity due to the multi-user interference of non-orthogonal MARC as Theorem 2 infers. The proposed PANC scheme with the power scaled factor can achieve full diversity no matter what power levels it adopts at relay node, which verify the proof of Theorem 2. The *Genie* method plays as the benchmark of the system performance, since it assumes that a genie exists at relay and guarantee that the relay transmit correct information to the destination. We can conclude from the simulation results that

the proposed PANC scheme with the design of allocating different power levels and adopting the power scaling factor can achieve full diversity in MARC system.

In addition, the SPER performance based on new coordinate is larger than the SPER based on original coordinate in low SNR (e.g., from 0dB to 5dB), and coincides after 10dB. The reason for such phenomenon is that the detector based on the new coordinate is sub-optimal comparing to the optimal ML detection in (3). Thus, the error performance based on the new coordinate is poorer than its counterpart based on the original coordinate. As the SNR grows, the minimum Euclidean distance between constellation points in both original and new coordinates increases. So the error performances become perfectly matched. The theoretically derived results of both original coordinate and transformed coordinate match the Monte-Carlo simulation results. It infers that the closed-form SPER expression is accurate by wedge error calculation method and the CT method.

Notice that, allocating different power levels at relay may vary the coding gain of the system. In particular, the SPER performance of optimized a and b based on the Maxmin method has the best coding gain for both original coordinate and CT case. It infers that our Maxmin is performance efficient and it has low complexity compared with exhaustive search. The SPER performance of random or fixed chosen a and b has poorer coding gain performance because they are not adaptive to the instantaneous CSI compared with the optimized a and b .

Since there exists error propagation from early source-relay hop to destination, we notice that the gap between the SPER performance of genie-aided PANC scheme and the SPER performance of original received constellation with optimized a and b is different with three relay location realization. In particular, such gap is quite small when we have a strong source-relay channel, and the gap becomes bigger as the relay moves further from source and closer to the destination. The reason is that with strong source-relay channel, the relay will generate more reliable information and thus degrades the influence of error propagation to destination.

VII. CONCLUSION

In this paper we propose a novel PANC strategy to minimize the system SPER by allocating different power levels to the network coded signals and achieve full diversity for a non-orthogonal MARC. Firstly, with the setup of IRC and IDC, respectively, we derive the decision regions for received signal and obtain the end-to-end SPER in closed form. Moreover, we propose a more efficient SPER derivation by transforming the parallelogram-shaped to the rectangle-shaped

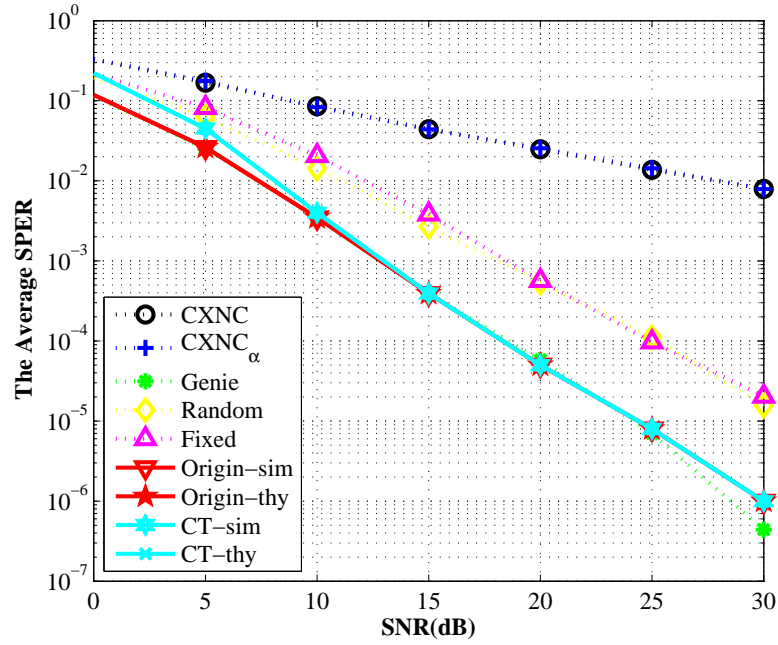


Fig. 5: Error performance with strong source-relay channel (Best viewed in color.).

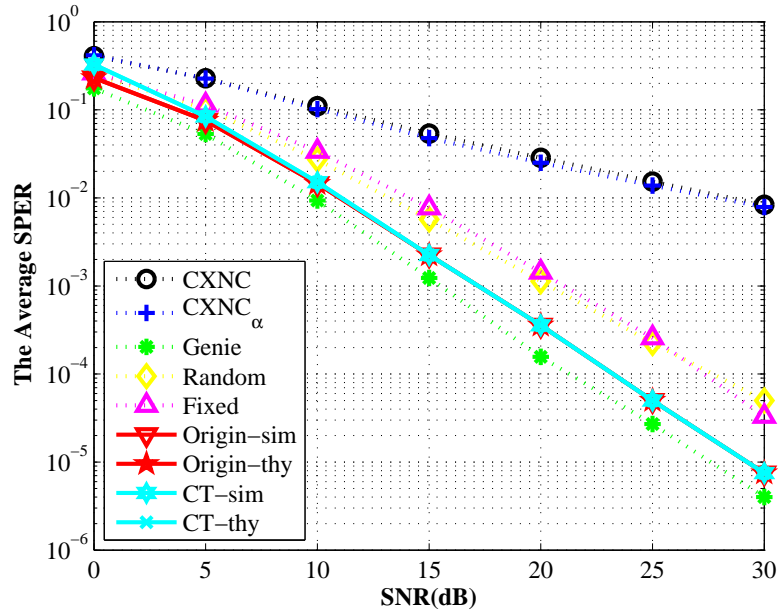


Fig. 6: Error performance in a symmetric network (Best viewed in color.).

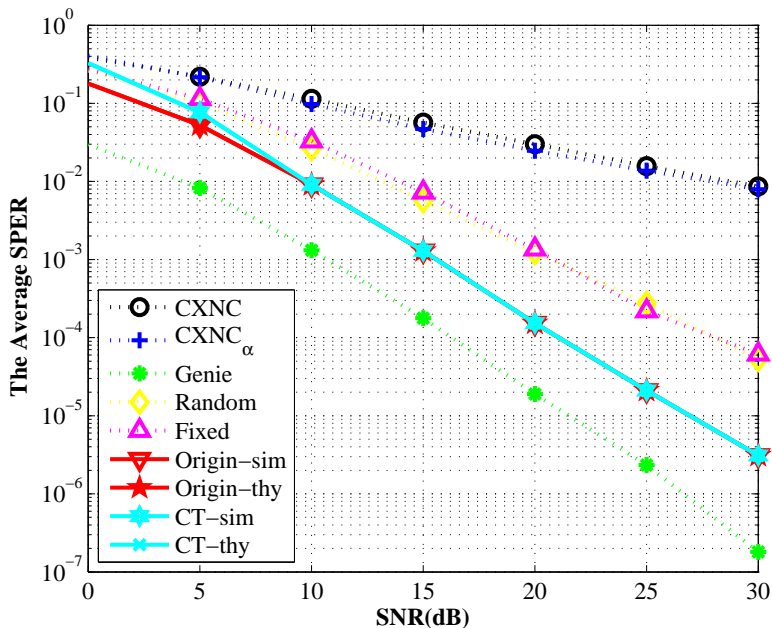


Fig. 7: Error performance with strong relay-destination channel (Best viewed in color.).

constellations, and therefore reduce the various derivations resulting from the randomization of channel conditions. By incorporating the power scaling method at relay, our proposed PANC scheme can achieve full diversity, which is proved in both theoretical and experiential aspects. In addition, to further minimize the error performance, we propose a max-min criteria based on the relationship between Euclidean distance and error probability, and formulate a convex optimization problem to obtain the optimal power adaption levels at relay. Simulations show that our method can achieve similar performances as genie-aided scheme and with low complexity. Simulation results show that the SPER derived based on our CT method can well approximate the exact SPER with a much lower complexity, and the PANC scheme with power level optimizations and power scaling factor design can achieve full diversity.

REFERENCES

- [1] T. Cover and A. Gamal, "Capacity theorems for the relay channel," *IEEE Trans. Inform. Theory*, vol. 25, no. 5, pp. 572–584, Sep. 1979.
- [2] J. N. Laneman, D. N. C. Tse, and G. W. Wornell, "Cooperative diversity in wireless networks: Efficient protocols and outage behavior," *IEEE Trans. Inform. Theory*, vol. 50, no. 12, pp. 3062–3080, Dec. 2004.
- [3] K. J. R. Liu, A. K. Sadek, W. Su, and A. Kwasinski, *Cooperative Communications and Networking*. Cambridge University Press, 2008.

- [4] R. Ahlswede, N. Cai, S. Y. R. Li, and R. Yeung, "Network information flow," *IEEE Trans. Inform. Theory*, vol. 46, no. 4, pp. 1204–1216, Jul. 2000.
- [5] S. Y. R. Li, R. W. Yeung, and N. Cai, "Linear network coding," *IEEE Trans. Inform. Theory*, vol. 49, no. 2, pp. 371–381, Feb. 2003.
- [6] S. Katti, H. Rahul, W. Hu, D. Katabi, M. Medard, and J. Crowcroft, "Xors in the air: practical wireless network coding," in *Proc. ACM SIGCOMM*, Sep. 2006, pp. 243–254.
- [7] T. Cui, T. Ho, and J. Kliewer, "Memoryless relay strategies for two-way relay channels," *IEEE Trans. Commun.*, vol. 57, no. 10, pp. 3132–3143, Oct. 2009.
- [8] S. Zhang and S. C. Liew, "Channel coding and decoding in a relay system operated with physical-layer network coding," *IEEE J. Select. Areas Commun.*, vol. 27, no. 5, pp. 788–796, Jun. 2009.
- [9] P. Popovski and H. Yomo, "The anti-packets can increase the achievable throughput of a wireless multi-hop network," in *Proc. IEEE International Conference on Communication (ICC 2006)*, vol. 9, Jun. 2006, pp. 3885–3890.
- [10] T. Koike-Akino, P. Popovski, and V. Tarokh, "Denoising maps and constellations for wireless network coding in two-way relaying systems," in *Global Telecommunications Conference, IEEE*, Dec. 2008, pp. 1–5.
- [11] —, "Optimized constellations for two-way wireless relaying with physical network coding," *IEEE J. Select. Areas Commun.*, vol. 27, no. 5, pp. 773–787, Jun. 2009.
- [12] G. Kramer, M. Gastpar, and P. Gupta, "Cooperative strategies and capacity theorems for relay networks," *IEEE Trans. Inform. Theory*, vol. 51, no. 9, pp. 3037–3063, Sep. 2005.
- [13] X. Bao and J. Li, "Adaptive network coded cooperation (ance) for wireless relay networks: matching code-on-graph with network-on-graph," *IEEE Trans. Wireless Commun.*, vol. 7, no. 2, pp. 574–583, Feb. 2008.
- [14] M. Xiao, J. Kliewer, and M. Skoglund, "Design of network codes for multiple-user multiple-relay wireless networks," *IEEE Trans. Commun.*, vol. 60, no. 12, pp. 3755–3766, Dec. 2012.
- [15] J. Li, J. Yuan, R. Malancy, M. Xiao, and W. Chen, "Full-diversity binary frame-wise network coding for multiple-source multiple-relay networks over slow-fading channels," *IEEE Trans. Veh. Technol.*, vol. 61, no. 3, pp. 1346–1360, Mar. 2012.
- [16] W. Guan and K. J. R. Liu, "Mitigating error propagation for wireless network coding," *IEEE Trans. Wireless Commun.*, vol. 11, no. 10, pp. 3632–3643, Oct. 2012.
- [17] J. Li, J. Yuan, R. Malaney, M. Azmi, and M. Xiao, "Network coded ldpc code design for a multi-source relaying system," *IEEE Trans. Wireless Commun.*, vol. 10, no. 5, pp. 1538–1551, May 2011.
- [18] M. Xiao and M. Skoglund, "Multiple-user cooperative communications based on linear network coding," *IEEE Trans. Commun.*, vol. 58, no. 12, pp. 3345–3351, Dec. 2010.
- [19] J. Craig, "A new, simple and exact result for calculating the probability of error for two-dimensional signal constellations," in *Military Communications Conference, IEEE*, vol. 2, Nov. 1991, pp. 571–575.
- [20] M. Karim, J. Yuan, Z. Chen, and J. Li, "Soft information relaying in fading channels," *IEEE Wireless Commun. Lett.*, vol. 1, no. 3, pp. 233–236, Jun. 2012.
- [21] S. Verdú, *Multiuser Detection*. Cambridge University Press, 1998.
- [22] A. Y. C. Peng, S. Yousefi, and I.-M. Kim, "On error analysis and distributed phase steering for wireless network coding over fading channels," *IEEE Trans. Wireless Commun.*, vol. 8, no. 11, pp. 5639–5649, Nov. 2009.
- [23] T. Wang, G. Giannakis, and R. Wang, "Smart regenerative relays for link-adaptive cooperative communications," *IEEE Trans. Commun.*, vol. 56, no. 11, pp. 1950–1960, Nov. 2008.
- [24] M. K. Simon and M. S. Alouini, *Digital Communication over Fading Channels*. Wiley-IEEE Press, 2004.
- [25] F. A. Onat, A. Adinoyi, F. Y., H. Yanikomeroglu, J. S. Thompson, and M. I. D., "Threshold selection for snr-based selective

digital relaying in cooperative wireless networks,” *IEEE Trans. Wireless Commun.*, vol. 7, no. 11, pp. 4226–4237, Nov. 2008.

APPENDIX

A. Computations on Wedge Probability

Wedge probability computation method in [19], [22] can be utilized to derive the SPER with irregular decision regions. In the following, we will discuss five wedge prototypes as shown in Fig. 8. Let us first review the wedges discussed in [22]. Denote the CP as V_i and vertex of wedge as M_k . Assume that the angle in counter-clockwise is positive and clockwise is negative, respectively.

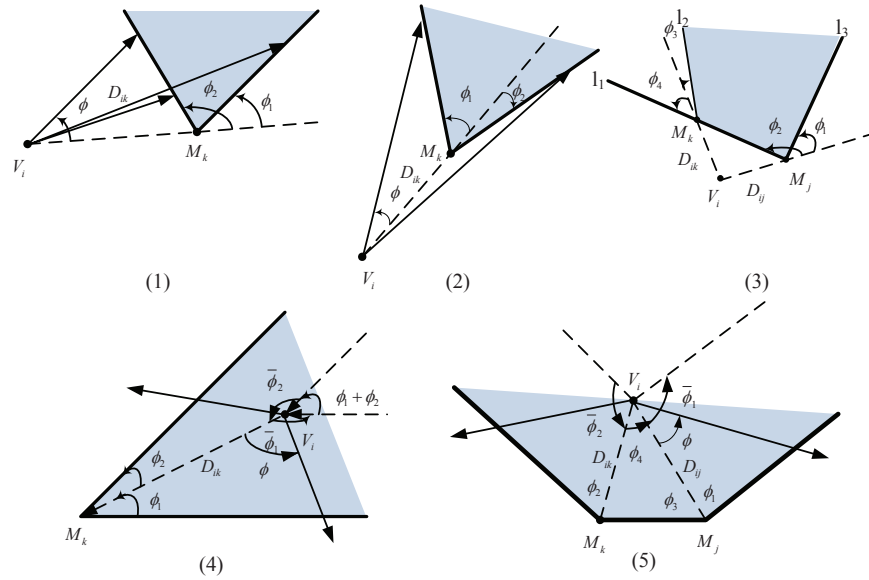


Fig. 8: Demonstrations for the basic patterns of wedge probabilities. d_{ik} (or d_{ij}) is the normalized distance between CP V_i and wedge vertex M_k (or M_j). In particular, both (1) and (2) are introduced in [22]; (3) is the wedge difference between wedge $l_1 - M_k - l_2$ and $l_1 - M_j - l_3$, denoted as $l_2 - M_k - M_j - l_3$, in which both l_1 and l_2 are sides of wedge $l_1 - M_k - l_2$, and l_3 is the side of wedge $l_1 - M_j - l_3$, respectively. And ϕ_i with $i \in \{1, \dots, 4\}$ are included angles between line $V_i M_k$ (or $V_i M_j$) and wedge side l_m for $m \in \{1, 2, 3\}$. In (4), ϕ_i with $i \in \{1, 2\}$ are included angle between line $V_i M_k$ and wedge sides; and $\phi_i + \bar{\phi}_i = \pi$. And in (5), ϕ_i with $i \in \{1, 2\}$ are included angle between line $V_i M_k$ and wedge sides; and $\phi_i + \bar{\phi}_i = \pi$; $\phi_3 = \angle V_i M_j M_k$ and $\phi_4 = \angle M_j V_i M_k$, respectively.

There are two types of wedge error probabilities to be considered when V_i is outside the

wedge region. For $\phi_1\phi_2 \geq 0$ as presented in Fig. 8 (1), the wedge probability is given by [22]

$$P_{w_1}(d_{ik}, \phi_1, \phi_2) = \frac{1}{2} \left\{ Q_2 \left(\sqrt{2d_{ik}} \sin \phi_2; \frac{\tan^2 \phi_2 - 1}{\tan^2 \phi_2 + 1} \right) - Q_2 \left(\sqrt{2d_{ik}} \sin \phi_1; \frac{\tan^2 \phi_1 - 1}{\tan^2 \phi_1 + 1} \right) \right\}, \quad (34)$$

where the two-dimensional Q-function $Q_2(x; \rho)$ is defined in Notations, and its closed-form solution can be found in Equation (5.74) on [24].

Similarly, for $\phi_1\phi_2 < 0$ as shown in Fig. 8 (2), the wedge error probability is shown as [22]

$$P_{w_2}(d_{ik}, \phi_1, \phi_2) = \frac{1}{2} \left\{ Q_2 \left(\sqrt{2d_{ik}} \sin \phi_1; \frac{\tan^2 \phi_1 - 1}{\tan^2 \phi_2 + 1} \right) - Q_2 \left(\sqrt{2d_{ik}} \sin(-\phi_2); \frac{\tan^2 \phi_2 - 1}{\tan^2 \phi_1 + 1} \right) \right\}. \quad (35)$$

Since decision regions may also be the difference of two wedges, for notational convenience, we introduce the probability involves difference between two wedges, as shown in Fig. 8 (3). According to the value of $\phi_1\phi_2$ and relative size of two wedges in Fig. 8 (1) and (2), we have error probability for wedge difference given as

$$P_{w_3}(d_{ij}, d_{ik}, \phi_1, \phi_2, \phi_3, \phi_4, m, n) = P_{w_m}(d_{ij}, \phi_1, \phi_2) - P_{w_n}(d_{ik}, \phi_3, \phi_4), \quad (36)$$

where $m, n \in \{1, 2\}$, angles ϕ_1 and ϕ_2 are with respect to vertex M_j , and angles ϕ_3 and ϕ_4 are with respect to vertex M_k .

Next, we discuss the probability of correct decisions, i.e., the received signal is inside the decision region of V_i . We use two different ways to represent the probabilities corresponding to two different decision regions, as shown in Fig. 8 (4) and (5). In particular, the probability of a received signal within the wedge region with vertex M_k , shown in Fig. 8 (4), is given by

$$\begin{aligned} P_{w_4}(d_{ik}, \phi_1, \phi_2) &= \frac{1}{2\pi} \sum_{n=1}^2 \left(1 - \int_0^{\bar{\phi}_n} \exp \left(-\frac{d_{ik} \sin^2 \phi_n}{\sin^2(\phi_n + \phi)} \right) d\phi \right) + \frac{\phi_1 + \phi_2}{2\pi} \\ &= \frac{1}{2\pi} \sum_{n=1}^2 \left(Q_2 \left(\sqrt{2d_{ik}} \sin \phi_n; \frac{\tan^2 \phi_n - 1}{\tan^2 \phi_n + 1} \right) - \pi Q_1 \left(\sqrt{2d_{ik}} \sin \phi_n \right) \right) + \frac{\phi_1 + \phi_2 + 2}{2\pi}. \end{aligned} \quad (37)$$

In addition, when the decision region of V_i is defined by a line segment M_jM_k and two rays with initial points M_j and M_k , respectively, shown in Fig. 8 (5), the probability of V_i inside such wedge combination is given by

$$\begin{aligned} P_{w_5}(d_{ik}, d_{ij}, \phi_1, \phi_2, \phi_3, \phi_4) &= \frac{1}{2\pi} \left\{ \sum_{n=1}^3 Q_2 \left(\sqrt{2d_{ij}} \sin \phi_n; \frac{\tan^2 \phi_n - 1}{\tan^2 \phi_n + 1} \right) - \sum_{n=1}^2 \pi Q_1 \left(\sqrt{2d_{ij}} \sin \phi_n \right) \right. \\ &\quad \left. - Q_2 \left(\sqrt{2d_{ik}} \sin(\phi_3 + \phi_4); \frac{\tan^2(\phi_3 + \phi_4) - 1}{\tan^2(\phi_3 + \phi_4) + 1} \right) + \phi_1 + \phi_2 + \phi_4 + 3 \right\}. \end{aligned} \quad (38)$$

B. Derivation of the coordinate transformation at relay

Define $\mathbf{Z} = [\Re\{y_{\mathcal{R}}\}, \Im\{y_{\mathcal{R}}\}]^T$ as the point on the original coordinate, where $(\cdot)^T$ is the transform operation of the matrix or vector, 2×1 vector \mathbf{Z}' as the intermediate transformed point, \mathbf{A} as the intermediate coordinate transformation matrix. The relationship between \mathbf{Z} and \mathbf{Z}' is $\mathbf{Z} = \mathbf{A}\mathbf{Z}'$, where \mathbf{A} is a 2×2 matrix and $\det(\mathbf{A}) \neq 0$. The probability density function of \mathbf{Z} can be represented by \mathbf{Z}' as

$$\begin{aligned} f_{\mathbf{Z}}(z) &= \frac{1}{2\pi|\Sigma|^{1/2}} \exp\left(-\frac{1}{2}(\mathbf{z} - \mathbf{V}_i)^T \Sigma^{-1} (\mathbf{z} - \mathbf{V}_i)\right) \\ &= \frac{1}{2\pi|\Sigma|^{1/2}} \exp\left(-\frac{1}{2}(\mathbf{z}' - \mathbf{A}^{-1}\mathbf{V}_i)^T \mathbf{A}^T \Sigma^{-1} \mathbf{A} (\mathbf{z}' - \mathbf{A}^{-1}\mathbf{V}_i)\right), \end{aligned} \quad (39)$$

where $\Sigma = [\sigma^2/2, 0; 0, \sigma^2/2]$, and $|\Sigma|$ is the determinant of Σ , $i \in \{1, \dots, 4\}$. Note that the covariance matrix $\mathbf{B} \triangleq \mathbf{A}^T \Sigma^{-1} \mathbf{A}$ is not diagonal, we adopt eigenvalue decomposition and obtain

$$f_{\mathbf{Z}}(z) = \frac{1}{2\pi|\Sigma|^{1/2}} \exp\left(-\frac{1}{2}(\mathbf{z}' - \mathbf{A}^{-1}\mathbf{V}_i^T)^T [\psi_1, \psi_2]^T \begin{bmatrix} \lambda_1 & 0 \\ 0 & \lambda_2 \end{bmatrix} [\psi_1, \psi_2](\mathbf{z}' - \mathbf{A}^{-1}\mathbf{V}_i^T)\right), \quad (40)$$

where ψ_i for $i = 1, 2$ and λ_i are the eigenvectors and eigenvalues of \mathbf{B} , respectively. Thus, we define $\bar{\mathbf{Z}} = [\psi_1, \psi_2](\mathbf{z}' - \mathbf{A}^{-1}\mathbf{V}_i^T)$, which is a complex Gaussian random variable with mean $\bar{\mathbf{V}}_i = [\psi_1, \psi_2]\mathbf{A}^{-1}\mathbf{V}_i^T$ and covariance $[\lambda_1, 0; 0, \lambda_2]$, as the point on the transformed coordinate. Let $\mathbf{Q} = [\psi_1, \psi_2]$, the relationship between original received signal \mathbf{Z} and the transformed received signal $\bar{\mathbf{Z}}$, original RP \mathbf{V}_i and transformed RP $\bar{\mathbf{V}}_i$ after coordinate transformation and decorrelation are

$$\bar{\mathbf{Z}} = \mathbf{Q}\mathbf{A}^{-1}\mathbf{Z} \quad \text{and} \quad \bar{\mathbf{V}}_i = \mathbf{Q}\mathbf{A}^{-1}\mathbf{V}_i^T, \quad (41)$$

respectively. To transform the RP-composed parallelogram to a rectangle centered at origin point and preserve the length of geometry's sides, e.g., $\overrightarrow{\bar{V}_i \bar{V}_j} = \overrightarrow{\bar{V}_i} \overrightarrow{\bar{V}_j}$, the transformation matrix \mathbf{A} is given by

$$\mathbf{A} = \begin{bmatrix} \overrightarrow{\bar{V}_1 \bar{V}_2} & -\overrightarrow{\bar{V}_1 \bar{V}_2} \\ \overrightarrow{\bar{V}_1 \bar{V}_3} & \overrightarrow{\bar{V}_1 \bar{V}_3} \end{bmatrix} \begin{bmatrix} \mathbf{V}_1(1) & \mathbf{V}_2(1) \\ \mathbf{V}_1(2) & \mathbf{V}_2(2) \end{bmatrix}^{-1} = \frac{2}{\beta} \begin{bmatrix} |h_{1\mathcal{R}}|\Im\{h_{2\mathcal{R}}\} & -|h_{1\mathcal{R}}|\Re\{h_{2\mathcal{R}}\} \\ -|h_{2\mathcal{R}}|\Im\{h_{1\mathcal{R}}\} & |h_{2\mathcal{R}}|\Re\{h_{1\mathcal{R}}\} \end{bmatrix}, \quad (42)$$

where $\beta = \Re\{h_{1\mathcal{R}}\}\Im\{h_{2\mathcal{R}}\} - \Re\{h_{2\mathcal{R}}\}\Im\{h_{1\mathcal{R}}\}$. And

$$\mathbf{B} = \frac{4}{\beta\sigma^2} \begin{bmatrix} |h_{1\mathcal{R}}|^2\Im^2\{h_{2\mathcal{R}}\} + |h_{2\mathcal{R}}|^2\Im^2\{h_{1\mathcal{R}}\} & -|h_{1\mathcal{R}}|^2\Re\{h_{2\mathcal{R}}\}\Im\{h_{2\mathcal{R}}\} - |h_{2\mathcal{R}}|^2\Re\{h_{1\mathcal{R}}\}\Im\{h_{1\mathcal{R}}\} \\ -|h_{1\mathcal{R}}|^2\Re\{h_{2\mathcal{R}}\}\Im\{h_{2\mathcal{R}}\} - |h_{2\mathcal{R}}|^2\Re\{h_{1\mathcal{R}}\}\Im\{h_{1\mathcal{R}}\} & |h_{1\mathcal{R}}|^2\Re^2\{h_{2\mathcal{R}}\} + |h_{2\mathcal{R}}|^2\Re^2\{h_{1\mathcal{R}}\} \end{bmatrix}, \quad (43)$$

And for $i = 1, 2$, the eigenvalues are shown as

$$\lambda_i = \frac{\mathbf{B}(1, 1) + \mathbf{B}(2, 2) \pm \sqrt{\mathbf{B}(1, 1)^2 + \mathbf{B}(2, 2)^2 + 4\mathbf{B}(1, 2)^2 - 2\mathbf{B}(1, 1)\mathbf{B}(2, 2)}}}{2}. \quad (44)$$

From (43) and (44) we can see that \mathbf{B} is a real orthogonal symmetric matrix. In this case, matrix \mathbf{Q} is a rotation matrix. Hence, the coordinate transformed by \mathbf{A} is a rectangle with its sides parallel to the axis, and after eigenvalue decomposition, the new constellation is still a rectangle and being rotated counterclockwise through an angle θ , which is defined by $\mathbf{Q} = [\cos(\theta), \sin(\theta); -\sin(\theta), \cos(\theta)]^T$. The corresponding eigenvectors matrix is given by (23). In this case, the final coordinate transform matrix \mathbf{C} is given by

$$\mathbf{C} = \mathbf{Q}\mathbf{A}^{-1}, \quad (45)$$

where \mathbf{A}^{-1} is shown in (23).

C. Proof of Theorem 1

Firstly, we consider the case that T_1 is wrongly decoded to other symbol pairs. The average probability that T_1 is wrongly decoded into T_4 at the destination is given by

$$\begin{aligned} P(T_1 \rightarrow T_4) &= \mathbb{E}\{P(T_1 \rightarrow T_4|\mathbf{h})\} \\ &= \mathbb{E} \left\{ \sum_{k \in \{\pm a, \pm b\}} P(T_1 \rightarrow T_4 | \sqrt{E_{\mathcal{R}}} x_{\mathcal{R}} = k, T_1, h_{1\mathcal{D}}, h_{2\mathcal{D}}, h_{\mathcal{R}\mathcal{D}}) P(\sqrt{E_{\mathcal{R}}} x_{\mathcal{R}} = k | T_1, h_{1\mathcal{R}}, h_{2\mathcal{R}}) \right\} \\ &= \mathbb{E} \left\{ Q_1 \left[\frac{\sqrt{2} \left(\left(\sum_{i=1}^2 \sqrt{E_i} |h_{i\mathcal{D}}| \right)^2 + |h_{\mathcal{R}\mathcal{D}}|^2 a^2 \right)}{\sqrt{(E_1 |h_{1\mathcal{D}}|^2 + E_2 |h_{2\mathcal{D}}|^2 + |h_{\mathcal{R}\mathcal{D}}|^2 a^2) \sigma^2}} \right] \left[1 - \sum_{i=1}^2 Q_1 \left(\sqrt{2} (E_i |h_{i\mathcal{R}}|^2 / \sigma^2) \right) \right. \right. \\ &\quad \left. \left. - Q_1 \left(\sqrt{2} \left(\sum_{i=1}^2 \sqrt{E_i} h_{i\mathcal{R}} \right) / \sigma^2 \right) \right] + Q_1 \left[\frac{\sqrt{2} \left(\left(\sum_{i=1}^2 \sqrt{E_i} |h_{i\mathcal{D}}| \right)^2 + |h_{\mathcal{R}\mathcal{D}}|^2 ab \right)}{\sqrt{(E_1 |h_{1\mathcal{D}}|^2 + E_2 |h_{2\mathcal{D}}|^2 + |h_{\mathcal{R}\mathcal{D}}|^2 a^2) \sigma^2}} \right] Q_1 \left(\sqrt{2} (E_1 |h_{1\mathcal{R}}|^2 / \sigma^2) \right) \right. \\ &\quad \left. + Q_1 \left[\frac{\sqrt{2} \left(\left(\sum_{i=1}^2 \sqrt{E_i} |h_{i\mathcal{D}}| \right)^2 - |h_{\mathcal{R}\mathcal{D}}|^2 ab \right)}{\sqrt{(E_1 |h_{1\mathcal{D}}|^2 + E_2 |h_{2\mathcal{D}}|^2 + |h_{\mathcal{R}\mathcal{D}}|^2 a^2) \sigma^2}} \right] Q_1 \left(\sqrt{2} (E_2 |h_{2\mathcal{R}}|^2 / \sigma^2) \right) \right. \\ &\quad \left. + Q_1 \left[\frac{\sqrt{2} \left(\left(\sum_{i=1}^2 \sqrt{E_i} |h_{i\mathcal{D}}| \right)^2 - |h_{\mathcal{R}\mathcal{D}}|^2 a^2 \right)}{\sqrt{(E_1 |h_{1\mathcal{D}}|^2 + E_2 |h_{2\mathcal{D}}|^2 + |h_{\mathcal{R}\mathcal{D}}|^2 a^2) \sigma^2}} \right] Q_1 \left(\sqrt{2} \left(\sum_{i=1}^2 \sqrt{E_i} h_{i\mathcal{R}} \right) / \sigma^2 \right) \right\}. \end{aligned} \quad (46)$$

Without loss of generality, we assume $E_1 = E_2 = E_{\mathcal{R}} = E$ in the following. Denote $\rho = E/\sigma^2$ as the reference system SNR for $i \in \{1, 2, \mathcal{R}\}$. In general, averaging the following one-dimensional Q-function over channel distributions, we have

$$\mathbb{E} \left\{ Q_1 \left(\sqrt{2\rho|h_{ij}|^2} \right) \right\} = \frac{1}{\pi} \int_0^{\pi/2} \left(1 + \frac{\rho\gamma_{ij}}{\sin^2\theta} \right)^{-1} d\theta \stackrel{\rho \rightarrow \infty}{\approx} \frac{1}{4\gamma_{ij}} \rho^{-1}. \quad (47)$$

Likewise, $\mathbb{E} \left\{ Q_1 \left(\sqrt{2\rho \sum_{t \in \{ij, mn\}} |h_t|^2} \right) \right\} \stackrel{\rho \rightarrow \infty}{\approx} \frac{3}{16\gamma_{ij}\gamma_{mn}} \rho^{-2}$ and $\mathbb{E} \left\{ Q_1 \left(\sqrt{2\rho \sum_{t \in \{ij, mn, pq\}} |h_t|^2} \right) \right\} \stackrel{\rho \rightarrow \infty}{\approx} \frac{5}{32\gamma_{ij}\gamma_{mn}\gamma_{pq}} \rho^{-3}$. According to the result shown in [25], we have the high-SNR approximation

$$\mathbb{E} \left\{ Q_1 \left[\frac{\sqrt{2} \left(\left(\sum_{i=1}^2 \sqrt{E_i} |h_{iD}| \right)^2 - |h_{\mathcal{R}D}|^2 ab \right)}{\sqrt{(E_1|h_{1D}|^2 + E_2|h_{2D}|^2 + |h_{\mathcal{R}D}|^2 a^2)} \sigma^2} \right] \right\} \approx \frac{\gamma_{\mathcal{R}D}}{\gamma_{1D} + \gamma_{2D} + \gamma_{\mathcal{R}D}}. \quad (48)$$

With the conclusion in (47) and (48), averaging the probability $P(T_1 \rightarrow T_4|\mathbf{h})$ in (46) over channel distributions, we further have

$$\begin{aligned} P(T_1 \rightarrow T_4) &\approx \frac{5}{32\gamma_{1D}\gamma_{2D}\gamma_{\mathcal{R}D}} \rho^{-3} + \frac{5}{128\gamma_{1D}\gamma_{2D}\gamma_{\mathcal{R}D}\gamma_{1\mathcal{R}}} \rho^{-4} \\ &+ \frac{\gamma_{\mathcal{R}D}}{4\gamma_{2\mathcal{R}}(\gamma_{1D} + \gamma_{2D} + \gamma_{\mathcal{R}D})} \rho^{-1} + \frac{\gamma_{\mathcal{R}D}}{4\gamma_{S\mathcal{R}}(\gamma_{1D} + \gamma_{2D} + \gamma_{\mathcal{R}D})} \rho^{-1}, \end{aligned} \quad (49)$$

where $\gamma_{S\mathcal{R}} = \gamma_{1\mathcal{R}} + \gamma_{2\mathcal{R}}$. Likewise, we can derive $P(T_2 \rightarrow T_3)$. When only one error occurs, we further have

$$P(T_1 \rightarrow T_2) \approx \begin{cases} \frac{3}{16\gamma_{1D}\gamma_{\mathcal{R}D}} \rho^{-2} + \frac{1}{4\gamma_{1\mathcal{R}}} \rho^{-1} + \frac{1}{4\gamma_{2\mathcal{R}}} \rho^{-1} + \frac{1}{4\gamma_{S\mathcal{R}}} \rho^{-1}, & \text{when } a > b, \\ \frac{3}{16\gamma_{1D}\gamma_{\mathcal{R}D}} \rho^{-2} + \frac{1}{4\gamma_{1\mathcal{R}}} \rho^{-1} + \frac{3}{64\gamma_{1D}\gamma_{\mathcal{R}D}\gamma_{2\mathcal{R}}} \rho^{-3} + \frac{3}{64\gamma_{1D}\gamma_{\mathcal{R}D}\gamma_{S\mathcal{R}}} \rho^{-3}, & \text{when } a < b, \\ \frac{3}{16\gamma_{1D}\gamma_{\mathcal{R}D}} \rho^{-2} + \frac{1}{4\gamma_{1\mathcal{R}}} \rho^{-1} + \frac{1}{16\gamma_{1D}\gamma_{2\mathcal{R}}} \rho^{-2} + \frac{1}{16\gamma_{1D}\gamma_{S\mathcal{R}}} \rho^{-2}, & \text{when } a = b. \end{cases} \quad (50)$$

Similarly, we can derive $P(T_1 \rightarrow T_3)$, $P(T_2 \rightarrow T_4)$. From (49), and (50), we can conclude that the PANC scheme can only achieve one order diversity in MARC system without power scaling.

In NC based MARC system, averaging the related PEPs over the channel coefficients, we have

$$\begin{aligned} P(T_1 \rightarrow T_4) &\approx \frac{5}{32\gamma_{SD}\gamma_{\mathcal{R}D}\gamma_{1\mathcal{R}}} \rho^{-3} + \frac{5}{32\gamma_{SD}\gamma_{\mathcal{R}D}\gamma_{2\mathcal{R}}} \rho^{-3} + \frac{1}{4\gamma_{SD}} \rho^{-1}, \\ P(T_1 \rightarrow T_2) &\approx \frac{3}{16\gamma_{1D}\gamma_{1\mathcal{R}}} \rho^{-2} + \frac{3}{16\gamma_{1D}\gamma_{2\mathcal{R}}} \rho^{-2} + \frac{3}{16\gamma_{1D}\gamma_{\mathcal{R}D}} \rho^{-2}. \end{aligned} \quad (51)$$

Similarly, we can derive $P(T_1 \rightarrow T_3)$, $P(T_2 \rightarrow T_3)$ and $P(T_2 \rightarrow T_4)$. In this case, we can conclude that the MARC system applied network coding cannot achieve full diversity.

D. Proof of Theorem 2

We prove Theorem 2 using our virtual channel model. After some manipulations, it is easy to show that given any power scaling coefficient α employed at the relay side, the lower bound of SPER can be in general approximated as

$$\begin{aligned}
P_v &\triangleq P((x_1, x_2, x_{\mathcal{R}}) \rightarrow (\hat{x}_1, \hat{x}_2, \hat{x}_{\mathcal{R}})) \\
&\approx \mathbb{E} \left[Q \left(\frac{(\sqrt{E_1}|h_{1\mathcal{D}}|(x_1 - \hat{x}_1) + \sqrt{E_2}|h_{2\mathcal{D}}|(x_2 - \hat{x}_2))^2 + \alpha|h_{\mathcal{RD}}|^2(x_{\mathcal{R}} - \hat{x}_{\mathcal{R}})^2}{\sqrt{E_1}|h_{1\mathcal{D}}|^2(x_1 - \hat{x}_1)^2 + E_2|h_{2\mathcal{D}}|^2(x_2 - \hat{x}_2)^2 + \alpha|h_{\mathcal{RD}}|^2(x_{\mathcal{R}} - \hat{x}_{\mathcal{R}})^2}} \right) \right] \\
&\stackrel{(x+y)^2 \leq 2(x^2+y^2)}{\leq} \mathbb{E} \left[Q \left(\frac{(\sqrt{E_1}|h_{1\mathcal{D}}|(x_1 - \hat{x}_1) + \sqrt{E_2}|h_{2\mathcal{D}}|(x_2 - \hat{x}_2))^2 + \alpha|h_{\mathcal{RD}}|^2(x_{\mathcal{R}} - \hat{x}_{\mathcal{R}})^2}{2\sqrt{(\sqrt{E_1}|h_{1\mathcal{D}}|(x_1 - \hat{x}_1) + \sqrt{E_2}|h_{2\mathcal{D}}|(x_2 - \hat{x}_2))^2 + \alpha|h_{\mathcal{RD}}|^2(x_{\mathcal{R}} - \hat{x}_{\mathcal{R}})^2}} \right) \right]. \tag{52}
\end{aligned}$$

After applying the Chernoff bound $Q_1(x) \leq \frac{1}{2} \exp\left(-\frac{x^2}{2}\right)$, we can further obtain

$$P_v \leq \mathbb{E} \left[\frac{1}{2} \exp \left(-\frac{(\sqrt{E_1}|h_{1\mathcal{D}}|(x_1 - \hat{x}_1) + \sqrt{E_2}|h_{2\mathcal{D}}|(x_2 - \hat{x}_2))^2 + \gamma_{\mathcal{SRD}}|x_{\mathcal{R}} - \hat{x}_{\mathcal{R}}|^2}{4} \right) \right] \stackrel{\rho \rightarrow \infty}{\approx} \frac{1}{2} \left(\prod_{k=1}^r \Lambda_i \right)^{-1} \rho^{-r} \tag{53}$$

where Λ_i , r are the i th non-zero eigenvalue and the rank of the diagonal matrix

$\left[\frac{(\sqrt{E_1}|h_{1\mathcal{D}}|(x_1 - \hat{x}_1) + \sqrt{E_2}|h_{2\mathcal{D}}|(x_2 - \hat{x}_2))^2}{4}, 0; 0, \frac{\gamma_{\mathcal{SRD}}(x_{\mathcal{R}} - \hat{x}_{\mathcal{R}})^2}{4} \right]$, respectively. $\gamma_{\mathcal{SRD}} = \min\{\gamma_{\mathcal{SR}}, \gamma_{\mathcal{RD}}\}$ is an exponential distributed random variable with mean $\frac{\gamma_{1\mathcal{R}}\gamma_{2\mathcal{R}}\gamma_{\mathcal{RD}}}{\gamma_{1\mathcal{R}}\gamma_{2\mathcal{R}} + \gamma_{1\mathcal{R}}\gamma_{\mathcal{RD}} + \gamma_{2\mathcal{R}}\gamma_{\mathcal{RD}}}$, which is proven as follows. Define $T = \min(E_1|h_{1\mathcal{R}}|^2, E_2|h_{2\mathcal{R}}|^2)$. Since $\gamma_{\mathcal{SRD}} = \min\{E_1|h_{1\mathcal{R}}|^2, E_2|h_{2\mathcal{R}}|^2, (\sqrt{E_1}|h_{1\mathcal{R}}| + \sqrt{E_2}|h_{2\mathcal{R}}|)^2, \gamma_{\mathcal{RD}}\}$, we have

$$2\gamma_{\mathcal{SRD}} \geq \min\{2E_1|h_{1\mathcal{R}}|^2, 2E_2|h_{2\mathcal{R}}|^2, E_1|h_{1\mathcal{R}}|^2 + E_2|h_{2\mathcal{R}}|^2, 2\gamma_{\mathcal{RD}}\} \geq 2 \min\{T, \gamma_{\mathcal{RD}}\}. \tag{54}$$

If X and Y are i.i.d. exponentially distributed random variables with mean v_x and v_y , respectively, $\min\{X, Y\}$ is also an exponentially distributed random variable with mean $v_x + v_y$. So we have the conclusion of $\gamma_{\mathcal{SRD}}$. Since both two diagonal elements are non-zero when an error event happens or two error events happen, we have $\max_{\hat{x} \neq x} \Pr(x \rightarrow \hat{x}) = O(\Gamma^{-2})$. Note that, replacing $\gamma_{\mathcal{RD}}$ in (53) by $\bar{\gamma}_{\mathcal{RD}}$ will not change the result of diversity, which completes the proof of the theorem.

If we apply the power scaling on CXNC scheme, when one error occurs, i.e., $\hat{x}_i = -x_i$ for $i \in \{1, 2\}$, we have

$$\begin{aligned}
&P((x_1, x_2, x_{\mathcal{R}}) \rightarrow (-\hat{x}_1, \hat{x}_2, \hat{x}_{\mathcal{R}})) \\
&\approx \mathbb{E} \left[Q \left(\frac{2E_1|h_{1\mathcal{D}}|^2}{\sqrt{E_1}|h_{1\mathcal{D}}|^2(x_1 - \hat{x}_1)^2 + E_2|h_{2\mathcal{D}}|^2(x_2 - \hat{x}_2)^2 + \alpha|h_{\mathcal{RD}}|^2(x_{\mathcal{R}} - \hat{x}_{\mathcal{R}})^2}} \right) \right]. \tag{55}
\end{aligned}$$

Averaging the probability in (55) over channel distributions, we further have

$$P((x_1, x_2, x_{\mathcal{R}}) \rightarrow (-\hat{x}_1, \hat{x}_2, \hat{x}_{\mathcal{R}})) \approx \frac{1}{4\gamma_{1\mathcal{D}}}\rho^{-1}. \quad (56)$$

Hence, we can conclude that the power scaled CXNC scheme still cannot achieve full diversity.